Report prepared by:
David Dukeman
Gray Mullins
Christopher L. Alexander

FINAL REPORT (Project BDV25-977-69)

Identification of the Mechanisms that Produce Hydrogen Embrittlement on Post-Tensioning Members and the Effects of Galvanic Coupling on Bridge Tendons

Final Report to Florida Department of Transportation

Christopher L. Alexander (PI)

Gray Mullins (Co – PI)

Timothy McCollough (FDOT Project Manager)

Tampa, FL 33620

April 2022

Disclaimer

The opinions, findings, and conclusions expressed in this publication are those of the authors and not necessarily those of the Florida Department of Transportation.

Universal Conversion Table

SI* (MODERN METRIC) CONVERSION FACTORS

APPROXIMATE CONVERSIONS TO SI UNITS

Symbol	When You Know	Multiply By	To Find	Symbol
		LENGTH		
in	inches	25.4	millimeters	mm
ft	feet	0.305	meters	m
yd	yards	0.914	meters	m
mi	miles	1.61	kilometers	km
		AREA		
in^2	square inches	645.2	square millimeters	mm^2
ft^2	square feet	0.093	square meters	m^2
yd^2	square yard	0.836	square meters	m^2
ac	acres	0.405	hectares	ha
mi^2	square miles	2.59	square kilometers	km^2
		VOLUME		
fl oz	fluid ounces	29.57	milliliters	mL
gal	gallons	3.785	liters	L
ft^3	cubic feet	0.028	cubic meters	m^3
yd^3	cubic yards	0.765	cubic meters	m^3
		NOTE: volumes greater than 1000 L shall be shown in m^3		
		MASS		
oz	ounces	28.35	grams	g
lb	pounds	0.454	kilograms	kg
T	short tons (2000 lb)	0.907	megagrams (or "metric ton")	Mg (or "t")
		TEMPERATURE (exact degrees)		
°F	Fahrenheit	5 (F-32)/9 or (F-32)/1.8	Celsius	°C
		ILLUMINATION		
fc	foot-candles	10.76	lux	lx
fl	foot-Lamberts	3.426	$candela/m^2$	cd/m^2
		FORCE and PRESSURE or STRESS		
lbf	poundforce	4.45	newtons	N
lbf/in^2	poundforce per square inch	6.89	kilopascals	kPa

APPROXIMATE CONVERSIONS FROM SI UNITS

Symbol	When You Know	Multiply By	To Find	Symbol
		LENGTH		
mm	millimeters	0.039	inches	in
m	meters	3.28	feet	ft
m	meters	1.09	yards	yd
km	kilometers	0.621	miles	mi
		AREA		
mm^2	square millimeters	0.0016	square inches	in^2
m^2	square meters	10.764	square feet	ft^2
m^2	square meters	1.195	square yards	yd^2
ha	hectares	2.47	acres	ac
km^2	square kilometers	0.386	square miles	mi^2
		VOLUME		
mL	milliliters	0.034	fluid ounces	fl oz
L	liters	0.264	gallons	gal
m^3	cubic meters	35.314	cubic feet	ft^3
m^3	cubic meters	1.307	cubic yards	yd^3
		MASS		
g	grams	0.035	ounces	oz
kg	kilograms	2.202	pounds	lb
Mg (or "t")	megagrams (or "metric ton")	1.103	short tons (2000 lb)	T
		TEMPERATURE (exact degrees)		
°C	Celsius	1.8C+32	Fahrenheit	°F
		ILLUMINATION		
lx	lux	0.0929	foot-candles	fc
cd/m^2	$candela/m^2$	0.2919	foot-Lamberts	fl
		FORCE and PRESSURE or STRESS		
N	newtons	0.225	poundforce	lbf
kPa	kilopascals	0.145	poundforce per square inch	lbf/in^2

*SI is the symbol for the International System of Units. Appropriate rounding should be made to comply with Section 4 of ASTM E380.

Technical Report Documentation Page

1. Report No.	2. Government Accession No.	3. Recipient's Catalog No.
4. Title and Subtitle Identification of the Mechanisms that Produce Hydrogen Embrittlement on Post-Tensioning Members and the Effects of Galvanic Coupling on Bridge Tendons		5. Report Date 4/2022 6. Performing Organization Code
7. Author(s) C. L. Alexander, D. Dukeman, G. Mullins		8. Performing Organization Report No.
9. Performing Organization Name and Address Department of Civil and Environmental Engineering University of South Florida (USF) Tampa, FL 33620		10. Work Unit No. (TRAIS) 11. Contract or Grant No. BDV25-977-69
12. Sponsoring Agency Name and Address		13. Type of Report and Period Covered Draft Final Report 4/1/20 – 4/30/22 14. Sponsoring Agency Code
15. Supplementary Notes		

16. Abstract

A preliminary analysis of failed prestressing strands within a post-tensioned tendon on the Wando River Bridge in South Carolina showed signs of possible hydrogen embrittlement. One proposed source of hydrogen is through galvanic coupling that may exist between the galvanized steel duct and the steel strands. This coupling, if present, can promote hydrogen evolution at the steel strand's surface, which may or may not be mitigated by the condition and quality of the grout. To fully understand the susceptibility of post-tensioned steel strands to hydrogen embrittlement in galvanized steel tendon ducts, this study set out to identify the conditions that promote hydrogen production, the kinetics of hydrogen evolution and adsorption into the steel, as well as the subsequent loss of strength of the steel strands.

17. Key Words: Prestressing Steel Wire, Failure Analysis, Corrosion, Grout segregation, Mechanical properties, Multiphysics simulations	18. Distribution Statement		
19. Security Classif. (of this report)	20. Security Classif. (of this page)	21. No. of Pages 73	22. Price

Form DOT F 1700.7 (8-72) Reproduction of completed page authorized

Acknowledgements

The authors would like to thank the South Carolina DOT for providing the failed tendon strands from the Wando River Bridge for our analysis.

Executive summary

A tendon failure on the Wando River Bridge in South Carolina sparked concern of the possibility of galvanic coupling-induced hydrogen embrittlement of the post-tensioned steel strands contained within galvanized steel ducts. The research presented in this work was focused on determining the conditions that promote galvanic coupling and its potential implications to tendon durability.

A literature review was performed focused on identifying the existing information available on the conditions that promote hydrogen production and the mechanisms of hydrogen embrittlement of cold-drawn pearlitic prestressing steels. Evidence was found of early galvanic action immediately following casting and lasting several days. Empirical relationships were identified that relate hydrogen content to reduction in fracture strength of the material.

A failure analysis was performed on fractured steel strands obtained from the Wando River Bridge provided by the South Carolina Department of Transportation (SCDOT). The results confirmed the role of corrosion in the failures but also identified absorbed hydrogen as a contributor. Because the tendon was mostly void of grout in the region of the failure, it is likely that the source of the hydrogen was the corrosion itself. However, if there was ever water present in the voided regions, substantial galvanic coupling could have occurred that may have accelerated the damage.

To identify the conditions that promote galvanic coupling between steel strands and galvanized steel ducts, experiments were performed on single wire mock tendons to quantify the amount of galvanic coupling as a function of grout condition. The grout condition was modified by either adding excess water while mixing or adding chlorides. The excess water resulted in grout segregation with regions of low pH and high sulfate concentration. In these regions, substantial corrosion of the galvanized steel duct was observed suggesting added galvanic coupling may have been possible. The most galvanic activity was measured within the first day after casting for the soft grout and chloride-contaminated conditions. Following the one-day exposure period, the resistivity of the grout began to increase, which resulted in substantial decreases in galvanic activity. The good grout condition did not promote enough galvanic activity to evolve hydrogen at any point during the exposure period. The results suggest that galvanic coupling is only a concern immediately after casting for improperly mixed grout. However, the results presented in this report are only reflective of a single grout formulation. The hydration behavior of other grout formulations reported in the literature may provide adequate information to suggest whether hydrogen absorption may be promoted in those cases.

A galvanic coupling model was formulated to simulate the level of galvanic activity for a typical tendon geometry considering the one-day exposure period data obtained from the single wire tendon experiments. The results were used to quantify the current density associated with the hydrogen evolution reaction to estimate the amount of hydrogen that may be produced considering conditions in which the imposed kinetic data was assumed not to change with time and oxygen was assumed to be plentiful such that depletion did not occur. It was found that the hydrogen evolution current density could be as much as 2.5 $\mu A/cm^2$ considering a 20-strand, 3-inch diameter tendon with a low grout resistivity which is reflective of a worst case scenario.

Autopsies of the mock tendons were performed to identify the amount of hydrogen that the wires absorbed, characterize the conditions of the grout in terms of chemical composition, pH, and physical

morphology. The soft grout conditions resulted in grout segregation with regions of low pH and high sulfate content as well as voids. There was substantial corrosion of the galvanized steel duct adjacent to the low pH regions of the grout. The chloride-contaminated grout also promoted duct corrosion, but it was more uniformly distributed. The chloride-contaminated condition also resulted in the most hydrogen absorption (0.9 ppm vs. 0.6 ppm for the good grout case).

Reverse bend tests were performed to assess the influence of the absorbed hydrogen on the steel ductility. Both the chloride-contaminated, and soft grout conditions resulted in decreased ductility. However, this test cannot be used to determine fracture strength. An empirical relationship identified through the literature was used to estimate the reduction in mechanical properties based on the measured corrosion potential and grout pH. These estimates suggested that the worst-case scenario was the very soft grout case in the low pH region, which results in a more positive standard hydrogen potential. While this result does not agree with the measured hydrogen content values, we can conclude that both chloride-contamination and excess water conditions would promote hydrogen absorption.

Therefore, based on the work presented, recommendation is made to adhere closely to the manufacturer's mixing specifications to ensure that grout segregation does not occur. Additionally, it is very important that the ducts are adequately sealed to prevent water intrusion. Further work is required to address the potential for oxygen depletion that may result in hydrogen absorption by the steel, to determine the role of sulfates in the absorption of hydrogen considering segregated and voided grout conditions, and to assess the feasibility and effectiveness of corrosion mitigation or rehabilitation methods.

Table of contents

List of Figures

List of Tables

1 Introduction

External post-tensioned tendons are used in segmental precast box girder bridge construction to hold segments together and prevent service cracking. The tendons consist of multiple 7-wire prestressing strands contained within a high-density Polyethylene (HDPE) duct located within the inner opening of the box girders. They run continuously through deviator blocks, which helps form the profile of the tendon. Within the deviator blocks, the ducts are made from a more rigid material such as galvanized steel. The ends of the tendon are anchored down at bulkheads and stressed, after which the duct is filled with cementitious grout [1]. The alkaline grout is intended to provide protection against corrosion, but due to voids in the grout and/or areas of improper mixing, cases of severe corrosion have occurred.

The corrosion of prestressing strands can have disastrous consequences if not detected early. More than 15 cases of corrosion in post-tensioned bridges have been reported in Florida alone. One of these cases is the Mid-Bay Bridge, which is 3.6 miles long and consists of 141 spans connecting Destin and Niceville, Florida. Corrosion of the prestressing strands was observed in areas of grout voids and bleed water and resulted in the replacement of several tendons [2]. Because the steel strands are contained within an HDPE duct and surrounded by grout, visual warnings are not apparent during the corrosion process.

Recently, a tendon failure on the Wando River Bridge in Charleston, South Carolina, resulted in subsequent damage of nearby structural components [3]. Metallurgical analysis performed by Applied Technical Services Inc. [4] reported that the failure was the result of loss in cross-sectional area and loss in flexibility due to corrosion. The authors stated that moisture ingress must be present to produce the localized corrosion observed. Analysis of the steel strands performed by the University of South Florida showed that some of the failed steel strands exhibited brittle like fracture, possibly the result of hydrogen absorption. Hydrogen content analysis performed by Luvak Inc. in Boylston, MA, reported that some of the steel strands had absorbed as much as 69 ppm of diffusible hydrogen, determined by vacuum pressure testing (inactive ASTM E 146-83), indicating that hydrogen embrittlement could be of serious concern [5].

Hydrogen is the lightest element and can dissolve in most metals and alloys through interactions with their crystal lattice [6]. Hydrogen atoms may freely move through a metal through the interstices of the crystal lattice or may become trapped at lattice defect sites. The ability of the trapped hydrogen to become released depends on the energy barrier of the defect. Defects with larger energy barriers make it more difficult for the trapped hydrogen to become released [7]. The absorbed hydrogen results in loss in plasticity through mechanisms which are still not fully understood. The loss in plasticity may result in cracks that can result in sudden material failure due to a brittle fracture. One potential source of the hydrogen is hydrolysis of corrosion products resulting in a low pH environment. Another source, and the focus of this work, is excessive cathodic polarization of the high strength steel as a result of galvanic coupling to the galvanized steel duct.

The objective of this investigation was to identify the possible consequences of galvanic coupling between the post-tensioned steel and the galvanized ducts in deviators and bulk heads with regards to the evolution of hydrogen on the high strength steel used for post-tensioning. To address the concern of hydrogen embrittlement within galvanized steel ducts, an analysis of failed tendon components obtained from the SCDOT and Florida Department of Transportation (FDOT) was performed, and the likelihood of hydrogen embrittlement of high strength steel strands under various grouting conditions was established through experiments and galvanic

coupling simulations. Chapter 2 of this report presents the results of a literature review focused on the mechanisms of hydrogen embrittlement and the conditions that promote it. Chapter 3 presents the results of the failure analysis of the Wando River Bridge tendon. Chapter 4 presents experimental results of the galvanic coupling experiments and established the influence of grout condition. Chapter 5 presents the implications of absorbed hydrogen on the mechanical properties of the prestressing steel. The conclusions of the work and recommendations for future research are presented in Chapters 6 and 7 respectively.

2 Literature Review

The following literature review was focused on organizing the existing information on the conditions that promote hydrogen production and the mechanisms of hydrogen embrittlement of cold-drawn pearlitic prestressing steels in an effort to determine the implications of grout conditions within galvanized steel ducts to prestressing steel failures. Information from prior failures of prestressing strands possibly the result of hydrogen embrittlement is used to uncover the conditions that may promote hydrogen production in post-tensioned tendons. Hydrogen damage (HD) is used by the European Structural Integrity Society (ESIS) in its TC10 Committee of EAC [7], but since the classical term of HE is common, we also use HE in this report.

2.1 Prior Evidence of Prestressing Failures Due to Hydrogen Embrittlement

A survey of 50 incidents of corrosion of prestressing steel in the United states was published in 1982 [8]. Of those failures, 10 were concluded to be probable cases of stress corrosion cracking (SCC), HE, or a combination of both. Most of the failures occurred in post-tensioned structures that were designed to be unbonded or without grout and a loss in ductility was attributed to exposure to an aggressive environment. In 2001, a worldwide survey of the performance of segmental and post-tensioned bridges in Europe was performed by the US Federal Highway Administration (FHWA) [9]. Out of 17,612 post-tensioned bridges only 2% reported tendon corrosion issues and there was only one mention of hydrogen embrittlement as a potential cause in Norway. Unfortunately, further details were not provided. Outside of the failures reported in these publications, two notable instances are described in detail below. One of the cases is the Berlin Congress Hall which represents one of the earliest known cases and the other a much more recent failure of a tendon on the Wando River Bridge.

2.1.1 Berlin Congress Hall

One of the earliest reported cases of HE of tendon strands goes back to Berlin Congress Hall in 1980. This structure comprised a double-curved roof made with prestressed concrete construction. Without any detected signs of failure initiation, the southern external roof suddenly collapsed. Based on failure analysis reports, the combined influences of design issues, construction errors, environmental conditions led to its collapse. Today, it is understood that St 145/160 prestressing steel which was used throughout the tendons was very sensitive to SCC [10]. This case provides some indication of the conditions that may promote HE within PT ducts. Wet conditions along with insufficient grouting of the tendons and poor quality concrete promoted hydrogen induced stress corrosion cracking of its tendons [11]. However, hydrogen content analysis of the failed strands was not performed. Interestingly, the strands were coated with a zinc-oxide to prevent corrosion prior to construction.

2.1.2 Wando River Bridge

The James B. Edwards Bridge runs over Wando River located in Charleston, South Carolina and was opened in 1989. A recent failure of one of the post-tensioned tendons occurred at a pier segment within a galvanized steel duct. At that location, the tendon was approximately 80% void of grout. During removal of the failed tendon, it was noted that 5 to 7 strands out of the total 19 strands were corroded [12]. The remaining grout pH was in some locations as low as 5. Metallurgical analysis performed by Applied Technical Services Inc. [3] reported that the failure was the result of loss in cross-sectional area and loss in flexibility due to corrosion. The authors stated that moisture ingress must be present to produce the

localized corrosion observed. Analysis of the steel strands performed by the University of South Florida showed that some of the failed steel strands exhibited brittle like fracture, possibly the result of hydrogen absorption. Hydrogen content analysis performed by Luvak Inc. in Boylston, MA, reported that some of the steel strands had absorbed as much as 69 ppm of diffusible hydrogen, determined by vacuum pressure testing (inactive ASTM E 146-83), indicating that hydrogen embrittlement (HE) could be of concern [4]. Whether the hydrogen was produced by galvanic coupling to the galvanize steel duct or though corrosion of the strands themselves requires further analysis.

In each of these failures, voids in the grout and wet conditions led to corrosion of the prestressing steel. In the Berlin Congress Hall case, failure was identified to be a result of hydrogen embrittlement due to the susceptibility of the steel. In the case of the Wando River Bridge failure, the corrosion of the strands was likely due to a combination of grout voids and water infiltration that resulted in some cases in brittle failures of the wires potentially enhanced by hydrogen absorption. It is not clear however, what the source of the hydrogen was and why the pH of the grout was so low. In the next sections, the manufacturing processes used to produce the prestressing wires is described as well as the existing knowledge on the mechanisms of hydrogen embrittlement and the relationships between hydrogen content and mechanical properties. Based on the information obtained, the implication of adverse conditions within galvanized steel tendons ducts to PT durability is assessed.

2.2 Cold Drawing of Steel Wires and its Effects on Microstructure

Prestressing strands comprise of seven high-strength steel wires in which 6 slightly smaller wires are helically wrapped around a single king wire. The wires are produced by a cold-drawing process in which the steel is pulled through multiple dies which successively reduces the size of the wires. The drawing process results in significant changes to the material's microstructure and therefore its mechanical properties.

The pre-drawn microstructure of the steel is of eutectoid composition and primarily composed of pearlite grains containing ferrite and cementite lamellae [13]. In general, the pearlite microstructural variations during the drawing process involve: (i) narrowing of the pearlite colonies; (ii) refinement of interlamellar spacing; (iii) and orientation of the lamellae towards the drawing direction. An interlamellar spacing in the range of tens of nanometers can be achieved by wire drawing [14]. The result is a high strength steel with a nanocomposite microstructure (pearlite colonies + pearlitic lamellae) in an oriented direction [15]. However, the general changes in the microstructural features during the drawing process may also be accompanied by site specific irregularities. The initial drawing steps primarily result in grain reorientation while further deformation primarily results in elongation and interlamellar spacing refinement [16]. The grain reorientation does not result in complete alignment of the lamellae and some of the grains are not realigned at all. In the case that the lamellae remain perpendicular to the drawing direction, the lamellae may become more spaced out and begin to kink. Additionally, dissolution of cementite and even breaking of the cementite lamellae can occur. These locations are considered weak points in the steel and are likely initiation sites of fracture.

Another outcome of the drawing process is residual stresses that are unevenly distributed throughout the cross section of the wires with the maximum stress at the surface of the wire. The residual tensile stresses cause the metallic bonds to be elongated resulting in excess space where small hydrogen atoms may diffuse through the steel more easily. If the number of drawing steps is increased, the residual tensile stresses will increase and hence increases the diffusivity of hydrogen atoms [17]. For this reason, the

ASTM standard requires a thermo-mechanical treatment step following the drawing process to obtain the desired mechanical properties [18]. Additionally, the residual stress can be partially controlled with the inlet die geometry [17]. The effect of residual stress formed by CD on HE is not considerable in low inlet die angle or high (more than wire radius) bearing lengths. CD with low inlet die angle and long bearing length will show high resistance to HE and therefore longer service life [19].

2.3 Proposed Mechanisms of Hydrogen Embrittlement

Johnson reported the decrease in the mechanical properties of metals due to the presence of hydrogen in 1875 [20] yet the mechanisms involved are still under investigation. Generally, there are two types of hydrogen embrittlement (HE). Internal hydrogen embrittlement (IHE) is due to the concentration of pre-existing hydrogen. Hydrogen environment embrittlement (HEE) involves cracking of metals under sustained loads in hydrogen containing environments. Environmental hydrogen embrittlement (EHE) is sometimes used for cathodically protected metals [21]. Heat treatments are the source for internal hydrogen, while external sources of hydrogen may include irradiation, pressurized hydrogen-gas, cathodic protection or corrosion in aqueous solutions. Prestressing steels do not have a substantial amount of internal hydrogen and therefore the information presented is focused on HEE in which the hydrogen is the result of the interaction of the steel with the environment.

Hydrogen molecules may be produced by hydrogen evolution as a result of the cathodic processes associated with the corrosion reaction or be driven electrochemically during cathodic polarization [22]. In the first stage of hydrogen evolution, hydrogen atoms adsorb on the metal's surface by discharging of hydrated protons or water splitting. Then, in the second stage, depending on the metal and the current density, the adsorbed hydrogen may desorb and form hydrogen molecules. Only a small amount of the adsorbed hydrogen is usually absorbed by the metal [23]. A summary of the reactions on the metal's surface when it is in contact with acidic solution according to the Volmer, Tafel and Heyrovsky routes are:

Volmer step: $H^+ + e^- \rightarrow H_{(ads)}$ Equation 2-1

Tafel step: $2H_{(ads)} \rightarrow H_2$ Equation 2-2

Heyrovsky step: $H^* + H_{(ads)} + e^- \rightarrow H_2$ Equation 2-3

Whereas, hydrogen evolution in alkaline media proceeds according to the following reactions:

Volmer step: $2H_2O + 2e^- \rightarrow 2H_{(ads)} + 2OH^-$ Equation 2-4

Tafel step: $2H_{(ads)} \rightarrow H_2$ Equation 2-5

Herovsky step: $H_2O + H_{(ads)} + e^- \rightarrow H_2 + OH^-$ Equation 2-6

Hydrogen in ferrous metals can be observed in three forms; 1- occupying interstitial sites (since H atom is very small) with a lattice distortion; 2- interacting with defects or adsorbing to the interfaces; 3- molecular hydrogen which forms by the recombination of atomic hydrogen resulting in micro-voids. The first two forms of hydrogen in the metal have high mobility, while the third one will lead to localized stresses. Hydrogen assisted cracking (HAC) is affected by different factors including hydrogen/surface reactions, hydrogen diffusion, and the degradation process of components. The microstructure of a component, temperature and strain rate are also among important studied parameters of HAC resistance [23].

Once hydrogen is absorbed into the metal, it will either diffuse through the lattice through interstitial sites or become trapped by lattice defects. At lower energy trap sites, the hydrogen may subsequently break free and continue to diffuse through the lattice structure. If the barrier energy is high, the hydrogen is said to be irreversibly trapped. Hydrogen-diffusion coefficients, D, usually are four to five orders of magnitude more in the case of body center cubic metals compared with face center cubic and hexagonal close packed metals at 20°C. It is also a temperature dependent parameter with stronger dependence for most hexagonal close packed metals. The hydrogen diffusion distance $\sim(2Dt)^{1/2}$

in body center cubic Fe with ($D \sim 10^{-5}$ cm^2/s) at 20°C is about 50 µm per second. HS steels usually have lower D-values mainly due to carbide phases and dislocation jungles. Hydrogen content in steels can be minimized by low-temperature heat treatment [21]. In addition, it is shown that hydrostatic stress distribution in H diffusion in pearlitic HS steels plays a significant role. The highest stress triaxiality in different notch geometries is related to the diffusion process. Toribio [24] developed equations showing H diffusion based on thermodynamic principles. It was revealed that H tends to move not only to the minimum concentration locations, but also to the maximum hydrostatic stress sites.

Several theories have been proposed to describe HE of high-strength low-alloy steels (HSLA). Hydrogen-enhanced decohesion (HEDE) was introduced in 1926 by Pfeil et al. [25] as a proposed mechanism. According to their theory, H decreases the cohesive metallic interatomic interactions and hence atoms become separated under low tensile stresses. Increasing H concentration will lead to decreasing of the metallic interatomic forces. The HEDE mechanism was confirmed by the observation of intergranular fracture and theoretical calculations. This mechanism is mainly proposed for HSLA steels with high levels of hydrogen concentration. Impurities in the grain boundaries such as phosphor or sulfur also will cause intergranular decohesion which promotes further hydrogen attraction and will accelerate the fracture.

In 1972, by careful study of hydrogen-assisted fracture surfaces, Beachem et al. [26] noticed tear ridges on brittle fracture surfaces and presented the hydrogen-enhanced localized plasticity HELP mechanism. In this mechanism, H accelerates dislocation formation and motion, resulting in local dislocation pileups with early failure of the material. This mechanism is based on the interaction between the H and dislocations. It was described to realize the effect of plasticity (as a result of dislocation motion) on the fractured samples. In contrast to the HEDE mechanism, plasticity of the alloy is important in HIC with the HELP mechanism. In 2004, Nagumo et al. [27] proposed that the absorbed H and vacancies both contribute to fracture failure and proposed the hydrogen enhancement of the strain-induced generation of vacancies (HESIV) mechanism. This mechanism assumes that H accelerates the development of strain-induced vacancies. As a result, formed vacancy clusters will lead to void initiation and growth causing early failure.

In recent years, the activation of HEDE and HELP mechanisms has been recognized by fractography of fractured surface and microstructural changes. Intergranular fracture or matrix/inclusion interface decohesion are signs of the HEDE mechanism, while HELP mechanism activates when HIC initiates from the intersections between slip bands. Researchers also observed mix brittle HIC surface features with microstructural evolution beneath intergranular fracture, suggesting a synergistic effect of HEDE and HELP mechanisms. This joint mechanism was also studied by statistical, physical-based and micro-mechanical models of HIC intergranular fracture in steels. In 2012, the nanovoid coalescence (NVC) mechanism was introduced [28] which describes the simultaneous effect of the HEDE, HELP and HESIV mechanisms. It is noteworthy that these mechanisms are based on the post-failure study of the samples, which cannot

provide direct evidence for the reduction in cohesive strength by H in the HEDE mechanism and for the propagation of dislocation motion by H in the HELP mechanism.

For pearlitic steels, HELP and HEDE are believed to be the primary embrittlement mechanisms. To determine which of HELP or HEDE is the major mechanism in HS steels, a micromechanical model of the fracture was developed by Toribio et al. [7]. Figure 2-1 shows the micromechanical model of HE in slightly CD steels with a tearing topography surface (TTS). This tearing mode can be described by the HELP mechanism and some degrees of plasticity. The appearance of the TTS mode looks like a ductile process similar to fatigue crack propagation, and it has been verified that the main crack growth mechanism during cyclic loading is plasticity-induced transfer of material from the crack tip to the apex [7].

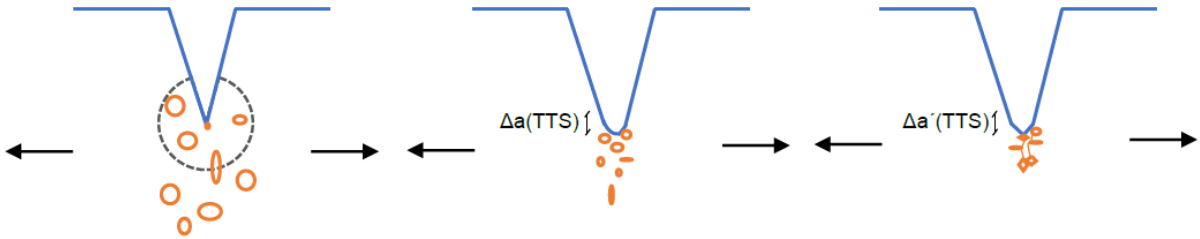

Figure 2-1. Micromechanical model of HD/HE in hot-rolled and slightly cold-drawn steels by HELP in the form of TTS, adapted from [7].

Figure 2-2 shows the micromechanical model of HE in HS steels with an intermediate degree of CD. Hydrogen diffuses at first inside the pearlitic microstructure. Then, HAC happens in the form of either trans-lamellar fracture path (HELP by Tearing Topography Surface) or by HEDE.

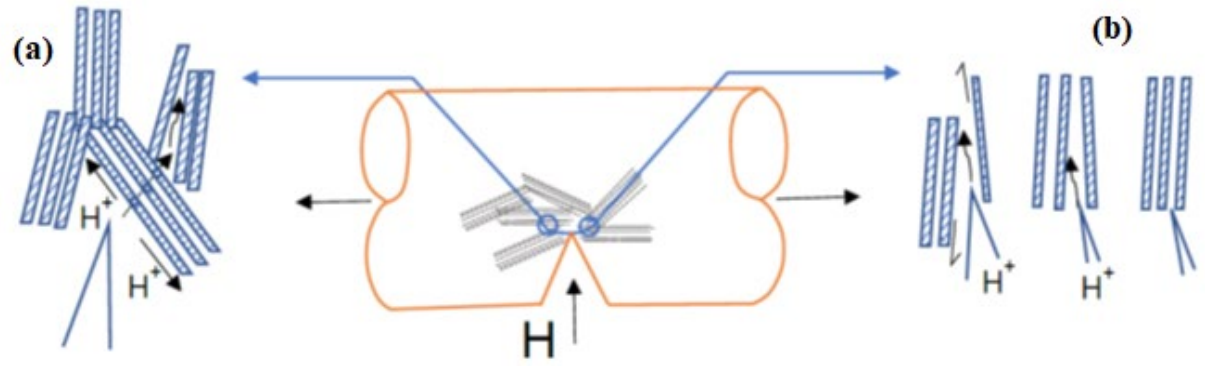

Figure 2-2. Micromechanical model of HE in steels with intermediate degree of CD: (a) hydrogen diffusion in the pearlite microstructure and trans-lamellar fracture path by TTS; (b) fracture by HEDE, adapted from [7].

During HE in heavily CD steels, hydrogen at first, diffuses through the preferential path parallel to the ferrite/cementite lamellae. Then, HAC occurs according to the HEDE mechanism. Factors causing the HE of CD steel resulting in a mixed elastic/plastic fracture mode were also investigated from the perspective of lattice defects. It was revealed that the number of lattice defects will not increase in the presence of H and under applying elastic stress and hence they are not a contributing factor to HE of CD pearlitic steel fractures in the elastic region, while they are the cause of the HE of CD steel that fractures in the plastic region [29].

2.4 Relationships Between Hydrogen Content and Mechanical Properties

While it is very difficult to relate the amount of hydrogen absorption a material experiences to its influence on macro-level mechanical properties, attempts to do so have been made. Barrera et al. [5] present a review of general relationships between the decay in mechanical properties due to HEDE and hydrogen content. In their review, they cite the work of Indeitsev et al. [30] which proposed a model for steels in general in which the fracture stress is related to the amount of hydrogen. They used an estimate based on the number of broken chemical bonds as a result of hydrogen presence. Their formula relates the H distribution by its chemical bonds and the plastic strain as:

$$\frac{n_0 - n_H}{n_0} = \frac{1}{1+\exp(\frac{\varepsilon_p - \varepsilon_0}{\varepsilon_c})} \quad \text{Equation 2-7}$$

where ε_p is plastic strain, ε_0 is the initial strain energy, ε_c is a fitting parameter, n_H is the number of hydrogen chemical bonds and n_0 is the total number of chemical bonds. According to the model, the flow stress (δ_Y), defined as the instantaneous stress required for further plastic deformation, decreases as the H concentration increases.

Another model presented which was developed specifically for pearlitic steels provides a relationship between the stress-strain response in the presence of hydrogen:

$$\sigma_Y = \frac{E\varepsilon_P}{1+(\frac{E}{E_H}-1)\frac{n_H}{n_0}} \quad \text{Equation 2-8}$$

where σ_Y is the flow stress, E is the Young's Modulus, and E_H is a fitting parameter. This equation shows that as the number of hydrogen chemical bonds increase, the flow stress decreases.

Enos et al. [31, 32] studied the effect of cathodic protection on hydrogen diffusion on pre-stressed tendons. They introduced a threshold concentration for hydrogen (C_{Hcrit}) which is defined as the critical diffusible H concentration below which, H does not affect fracture initiation. They estimated this value to be around 2×10^{-7} mol/cm^3 for prestressing steel. Reaching this concentration will lead to reduction of the axial fracture-initiation stress which was obtained for a bluntly notched HS steel. They also performed a series of constant-extension-tensile tests (CERT) and by interpolating the results, introduced a general relationship between diffusible H concentration (in lattice + weakly trapped) (C_H) and the local fracture-initiation strain:

$$\sigma_{eff}^{f} = \sigma_{air} - \alpha \log(C_H/C_{Hcrit}) \quad \text{Equation 2-9}$$

In this formula, σ_{eff}^{f} represents the local fracture-initiation stress.

Hartt et al. [33] introduced a criterion based on applied potential for cathodically protected tendons. However, it seems that as the pH of the steel/concrete at the interfacial zone may vary with the position of tendons inside the pile or duct, introducing a general potential for hydrogen production may not be precise enough to ensure both satisfactory CP and prevention of hydrogen production.

2.5 Implications to Grouted Post-Tensioned Tendons

Structures incorporating post-tensioned tendons (PTT) are expected to have a service life of many decades but, often need rehabilitation within several years of service due to corrosion. Corrosion in many cases has occurred in regions of grout deficiencies in the form of voids formed by bleed water accumulation and subsequent reabsorption or evaporation through incomplete anchorage sealing. Other possible causes of corrosion include intrusion of external chloride and water through anchorages or defects in the HDPE and possible adverse galvanic coupling between anchorage components and the strand. In some cases, corrosion of the steel may be accompanied by hydrogen absorption and subsequent embrittlement resulting in brittle failure [34].

General corrosion usually does not affect the load bearing capacity of the strands. However, prestressing steel faced with localized corrosion (such as pitting), may loose it's load bearing capacity and fail in a brittle fashion. The local pH-value within a pit will decrease due to hydrolysis of the Fe^{2+} ions. When sensitive prestressing steel is exposed to a chloride-containing media, the presence of hydrogen can lead to serious damage. Hence, in such cases, all types of localized corrosion should be prevented.

In establishing the susceptibility of a system to hydrogen embrittlement, the sources of hydrogen, its absorption and transport rates, and the influence on mechanical performance need to be identified. According to the two failures presented in this paper, voided tendon ducts seem to play a primary role to the failure modes. While hydrogen is not usually present in the environment within post-tensioned ducts, hydrogen uptake by prestressing steels in voided regions has been reported. Fernandez et al. [34] measured the amount of hydrogen uptake by stressed steels in voided ducts similar to the construction period following placement, of the strands and prior to grout placement which in some cases can be a couple of weeks. Strands contained within closed voided ducts with water showed a much higher hydrogen content than strands contained within closed dry ducts. Additionally, Hartt et al. [33] showed that within galvanized steel ducts, as used in the Wando River Bridge at the site of failure, hydrogen is cathodically produced immediately following grouting at the strand surface due to galvanic coupling to the galvanized duct immediately following grouting. The authors suggested that enough hydrogen is produced during this time to potentially cause embrittlement. However, the amount of hydrogen that was absorbed into the steel during the period immediately following grouting was not measured. Immediately following placement of the grout, the grout is wet and has a high conductivity, which promotes galvanic action between the galvanized duct and the steel strands. As the grout cures, the coupling diminishes. Based on this information, the question arises of what may occur if aggressive water infiltrates the galvanized steel tendon duct, potentially resulting in a highly conductive grout.

Pereira [35] evaluated the corrosion protection of bonded internal tendons in precast segmental construction at segment joints with either dry or sealed joints. They showed that the galvanized steel ducts were susceptible to severe corrosion in the case of a dry segment joint. Some of their results showed complete corrosion of the galvanized duct. Although concrete coverage was found to be less than allowed by specifications, results revealed the potential corrosion damage possible in the case of galvanized steel ducts in the presence of aggressive media. The concern is that water infiltration into the tendon duct may produce conditions similar to those present immediately following placement of the grout, where it has been determined that hydrogen evolution occurs on the strand surface.

Tendon ducts are constructed in some cases with galvanized steel for corrosion protection when cast into concrete structural elements. However, studies during the recent decade showed that applications of galvanized steel post-tensioning ducts provide limited corrosion protection for internal tendons (tendons cast into the concrete structure). These ducts may corrode through exposure conditions or by low

concrete cover [36]. Direct contact between galvanized surfaces and prestressing steel has been reported as a cause of damage in some cases [37]. The damage mechanism depends on different parameters (e.g., prestressing level, susceptibility to stress corrosion cracking, temperature, etc.). According to the DIN 1045-1 standard (no longer in use), prestressing steel should not be electrically connected with parts made of galvanized steel and should be separated by a minimum distance of 2 mm. However, the distance between steel and zinc does not have significant influence on the polarization of the steel, while the area (steel: zinc ratio) significantly affects it (critical area ratio of 10:1). Indirect contact between prestressing steels and galvanized surface is not critical; however, direct contact must be avoided [37].

If conditions are present that promote hydrogen production, even if the absorbed hydrogen does not lead to substantial material embrittlement, they may have an influence on the corrosion resistance of the material. Absorbed hydrogen has been shown to influence the stability of the passive film and also result in increased corrosion rates [38]. On passive metals, the H atoms diffuse through the passive film, reduce the O^{2-} ions to OH^- ions, and OH^- ions to H_2O molecules. These products may exchange with the Cl^- ions, if present, and destabilize the passive film. Also, the presence of hydrogen may cause a reduction in the stability of the passive film and may result in a decrease in the thickness of the passive film. In non-passivation solutions, adsorbed hydrogen can also increase the corrosion rate of steels. The potential impact of hydrogen on corrosion rate of these steels may be influenced by several factors including decohesion of metallic bonding, increasing mobility of dislocations, hydrogen-induced phase transformation, and also formation of vacancies in metallic lattice [6].

2.6 Summary

One of the earliest cases of hydrogen embrittlement of prestressing strand was the Berlin Congress hall failure. More recently, the presence of high hydrogen concentrations were reported in the failed strands of a post-tensioned tendon on the Wando River Bridge in which the duct was made of galvanized steel. In both of these cases, insufficient grouting and wet conditions promoted corrosion and potentially hydrogen embrittlement. However, in each case it has not been identified what the exact mechanism of hydrogen production or hydrogen absorption was that led to embrittlement.

There has been prior evidence that the possibility of galvanic coupling between steel and galvanized structural components could promote hydrogen production. Therefore, high conductivity grout either a result of improper mixing or water intrusion may promote hydrogen embrittlement. In the case that voids are present in the grout leaving the steel strand unprotected, hydrogen absorption could occur through corrosion process or previously absorbed hydrogen could enhance corrosion activity.

With the numerous studies that have been performed to understand the mechanisms of HE, multiple theories now exist. Some of the possible mechanisms of HE of pearlitic HS steels are hydrogen-enhanced decohesion (HEDE), hydrogen-enhanced localized plasticity (HELP), and hydrogen-enhanced strain-induced vacancies. In the case of moderately cold-drawn pearlitic steel, both the HELP and HEDE mechanism may occur.

While relationships have been developed to describe the change in mechanical properties due to hydrogen absorption and diffusion of steels in general, only one has been proposed specifically for cold-drawn pearlitic steels and is based on empirical data. Enos et al [8] propose a logarithmic relationship between diffusible hydrogen concentration and the local fracture-initiation strain. Additionally, a

threshold concentration for hydrogen around 2×10^{-7} mol/cm^3 was reported at which above this concentration, the axial fracture-initiation stress is expected to reduce.

3 Failure Analysis

Recently in November of 2016, a tendon failure on the I-526 James B. Edwards Bridge, also known as the Wando River Bridge (WRB), in Charleston, South Carolina resulted in subsequent damage of nearby structural components[39]. The bridge was built in 1989 across the Wando River[40] and is constructed from 51 segmental post-tensioned box girder spans and spans 7,900 feet. While the tendon was removed, it was noted that 5 to 7 strands showed signs of severe corrosion[40, 41]. Metallurgical analysis performed by Applied Technical Services, INC[42]. reported that the failure was the result of loss in cross-sectional area and loss in flexibility due to corrosion. The authors stated that moisture ingress must be present to produce the localized corrosion observed. Analysis of the steel strands performed by the University of South Florida showed that some of the failed steel strands exhibited brittle like fracture, possibly the result of hydrogen adsorption. Hydrogen content analysis performed by Luvak Inc. in Boylston, MA reported that some of the steel strands had absorbed as much as 69 ppm of diffusible hydrogen determined by vacuum pressure testing (inactive ASTM E 146-83) indicating that hydrogen embrittlement could be of serious concern[43]. Whether the source of hydrogen could have been due to galvanic coupling between the galvanized steel duct and the steel strands is one of the focuses of this project.

In this chapter, a more detailed failure analysis is presented of failed post-tensioned strands obtained from the Wando River Bridge to identify the primary source of hydrogen that resulted in brittle fractures of some of the strands. The failure analysis comprised inspection of the fracture morphology, quantification of hydrogen concentration as well as the reduction in cross-sectional area due to corrosion. The degree of corrosion was related to the expected reduction in strength to evaluate the likelihood of failure due to corrosion versus hydrogen embrittlement.

3.1 Methods

Two sections of the failed tendon were obtained from the South Carolina DOT according to the diagram presented in Figure 3-1. One of the sections included one end of the failed or broken strands that were contained within the galvanized duct of the pier diaphragm and the other section was taken from the external portion of the tendon. The focus of this report is the analysis of the failed section.

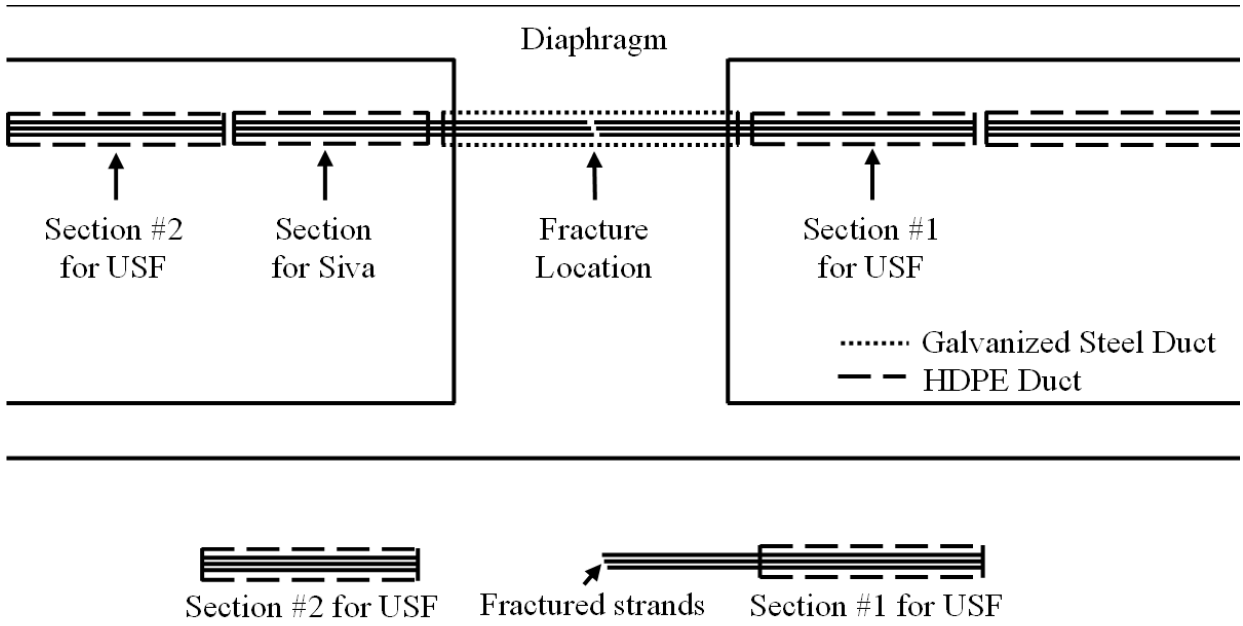

Figure 3-1. Failed tendon cut scheme.

A visual analysis was performed of the fractured ends of the strands to assess the surface for indications of brittle or ductile failure. All wires of each of the 19 strands were unwound and imaged. The locations of the individual fractured wires with respect to the cross-section of the strand was noted. For individual wires, visual signs of necking and cup and cone formation at the fracture end were recorded as a sign of ductile behavior. In contrast, individual wires with no visual signs of necking and no discernable cup and cone formation were recorded as brittle behavior. Additionally, the individual wires at the fractured end were inspected for signs of metal loss due to corrosion. Visual indications of corrosion could be grouped into three categories, no corrosion, mild corrosion, and moderate corrosion.

Microstructural analysis was performed on selected wires to identify the presence of microcracks indicative of embrittlement. Before performing the analysis, the selected samples were cut to size using a slow speed cutting saw and a non-corrosive cutting fluid to minimize temperature fluctuations during cutting. The samples were then attached to a sample holder and lightly plated using a gold/palladium sputter. Scanning electron micrographs were obtained of the fracture surface and the adjacent longitudinal surface.

The corrosion morphology near the fractured ends was assessed using a high resolution 3-D surface scanner. The objective was to quantify the loss in cross sectional area due to corrosion. To do this, any reduction in area due to plastic deformation (necking) had to be accounted for. The average reduced necking area was determined by fitting a circle to the partial necking that was visible in the cross-sectional view as seen in Figure 3-2 right. After identifying the reduced area due to necking, A_n, the uncorroded fracture surface area, A_r, was identified as shown in Figure 3-2 middle. The degree of corrosion is then calculated as

$$\text{Degree of Corrosion } (\%) = \frac{A_n - A_r}{A_n}\ x\ 100 \qquad \text{Equation 3-1}$$

While it can be expected that necking results in an observably reduced fracture surface area, it is assumed that the percentage of cross section loss due to corrosion is the same whether necking was present or not.

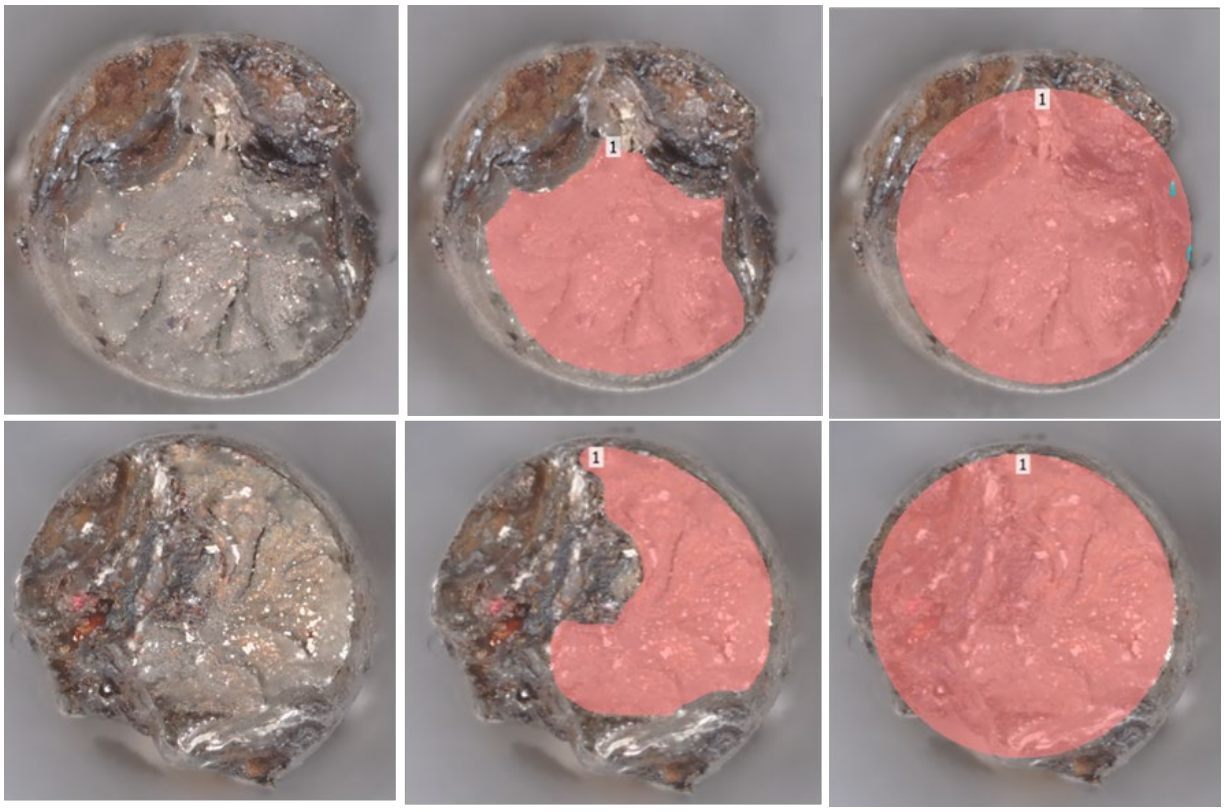

Figure 3-2. Cross-sectional view of selected samples (left), measured non-corroded area (center) and reduced necking area (right).

In addition to the quantitative measurement of the amount of surface corrosion in the cross-section of the fracture, a qualitative analysis on the outer surface of the wire near the fracture was performed. To observe the severity of pitting, the selected samples were first sandblasted to remove any surface corrosion and then imaged using 3D profilometry. In this way the corrosion morphology may be observed which may provide an indication of what may have caused the damage.

After careful inspection of the failed wires, 10 wires were selected from multiple strands for hydrogen content analysis based on their failure modes as determined by the visual analysis. These wires were sandblasted to remove any surface corrosion products, imaged to determine the severity of the corrosion, and then sent out for hydrogen content. The hydrogen testing was conducted by Luvak Inc. who performed a vacuum hot extraction (ASTM E 146-83) to determine the total amount of absorbed hydrogen. While the results obtained in this way may not be extremely accurate, the information obtained may be used on a comparative level.

3.2 Results

The observations made by the visual inspection are presented in Table 1. All of the strands obtained and analyzed were fractured. Some of the strands had a white residue on their surface that was likely a

byproduct of the grouting process. Interestingly, the wires that fractured in a ductile manner tended to have the least amount corrosion while wires seeming to have failed in a brittle manner were the most corroded. Out of the 102 wires examined only 24 (23.5%) of wires showed signs of ductile fracture behavior as indicated by substantial necking prior to fracture and a cup and cone fracture pattern as shown in Figure 3-3a. The remaining 78 wires either showed completely brittle fractures (64) or a combination of ductile and brittle behavior (14). An example of a brittle fracture surface is shown in Figure 3-3b.

Table 1. Compiled results from visual inspection and surface profilometry techniques.

Form of Failure	No Necking	Light Necking	Cup/Cone Necking	Shear Crack	No Corrosion	Mild Corrosion	Moderate Corrosion	Total wires
Ductile	0	12	11	14	3	20	1	24
Brittle	52		0	51	0	36	28	64
Ductile/ Brittle	0	14	0	13	0	12	2	14
Total	52	39	11	78	3	68	31	102

A)  B) 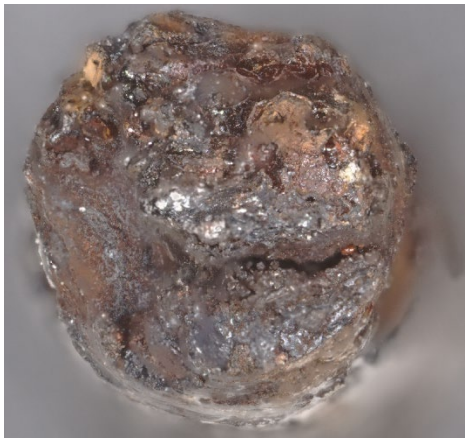

Figure 3-3. Example of (A) ductile failure with partial cup/cone fracture pattern; (B) brittle failure.

Ideally, as the tensioned high-strength steel strands are stressed beyond their yield strength, the individual wires will start to neck. The necking process occurs gradually at first and once the cross-section of the strand becomes reduced, the rate of necking will increase. The delayed behavior of ductile necking fracture allows for the tensile stresses to be redistributed from the necking wire to other neighboring wires in the same strand. In contrast, when the tensioned high-strength steel strands undergo brittle fracture behavior, the individual wires will fracture abruptly, often leading to neighboring wires to fracture near each other. Figure 3-4 shows an example of wires failing in different locations along a single strand. 51% (52/102) of the fractured wires showed no visual signs of necking and resembled a brittle failure mode. Only 10.8% (11/102) of wires showed good cup/cone ductile behavior. In general, the wires that showed ductile behavior had clear necking at the fracture and mild to no corrosion near the fracture. 54.5% (6/11) of the ductile wires that showed good cup/cone behavior were king wires.

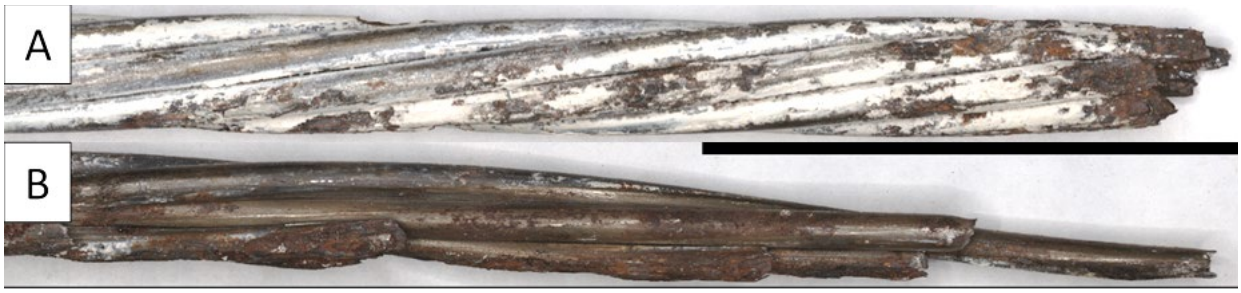

Figure 3-4. Example of (A) a strand with brittle fractures on all wires and (B) a strand with a combination of ductile and brittle fractured wires.

Additionally, it was noted that on ¾ of the strands, a fracture surface that was oriented at a slight angle to the longitudinal axis of the wires was present. An example of this is shown in Figure 3-5. The smooth surface resembles a shear cracking plane normally observed at a 45-degree angle to the orientation of maximum tensile stress. The winding of the wires around the king strand could have resulted in shear cracks at a slightly different angle but confirmation of this is required. Shear cracking generally occurs due to excessive shear stress applied to a slip plane during yielding of the steel.


Figure 3-5. Example of a single wire with shear cracking at the fracture end.

Another visible feature associated with some of the brittle failures was the presence of cracks at the fracture surface progressing longitudinally into the fracture plane and along the length of the wire. An example may be observed in the micrograph presented in Figure 3-6. These microcracks were viewed on the fracture surface of the wires however, other microcracks were also found on the side of some wires. According to[44], as the hydrogen content within the wires increases, the extent of longitudinal splitting increases and the fracture surface becomes more tortuous. Therefore, the microcracks observed are a good indication of hydrogen embrittlement.

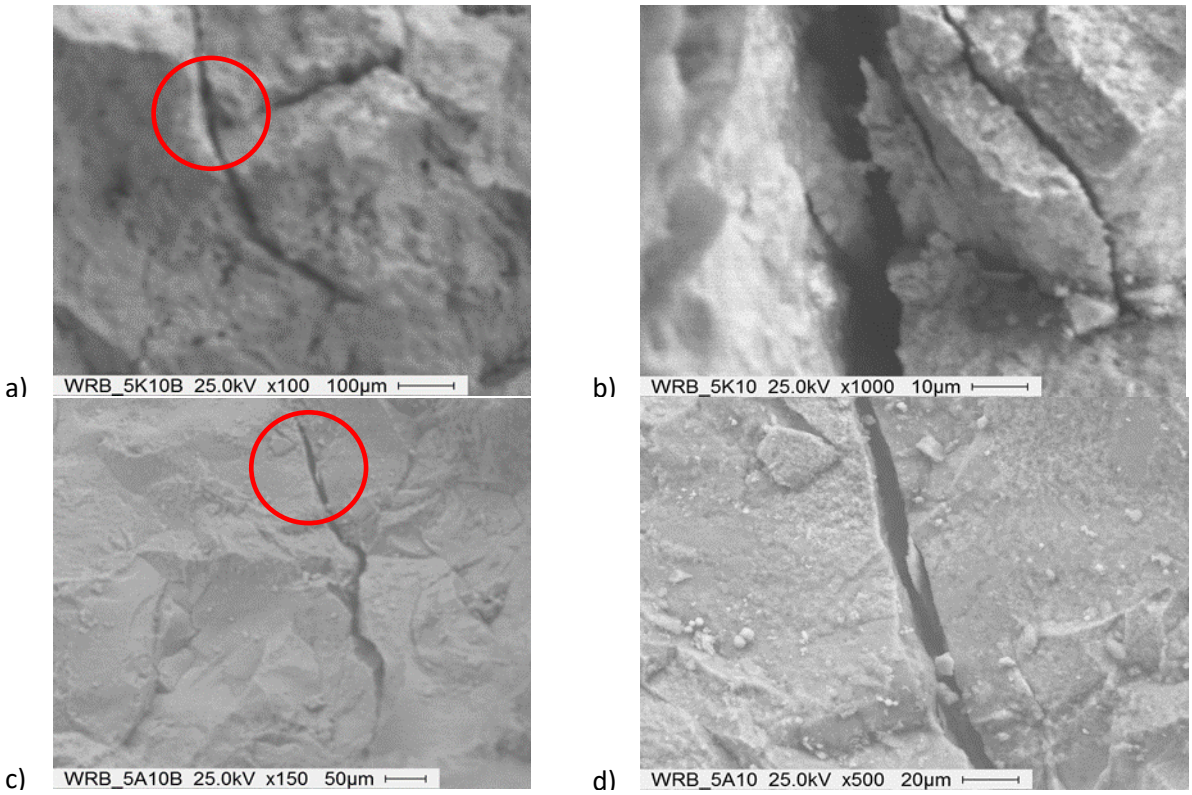

Figure 3-6. SEM images of a microcrack on a brittle wire. Images (B) and (D) are taken at higher magnifications at the circled areas of the cracks seen on images (A) and (C), respectively.

While the fracture patterns clearly show indications of embrittlement, they do not necessarily reveal their cause. Embrittlement can occur under excessive cathodic polarization or it can be induced by corrosion. Based on the results provided in Table 1, 97.1% (99/102) of wires examined showed some signs of corrosion, whether it be mild or moderate, leaving only 2.9% (3/102) of wires showing no signs of corrosion. An example of each degree of corrosion can be seen in Figure 3-7. In general, most of the wires observed experienced mild uniform surface (Figure 7b) corrosion near the fractured end of the strand. In some cases, moderate corrosion was observed in more localized areas in the form of significant metal loss. Only a few of the wires did not have visible signs of corrosion near the fractured end.

Figure 3-7. Example of (A) strands that have no corrosion, (B) mild corrosion, and (C) moderate corrosion.

By comparing the fracture mode to the level of corrosion present near the fracture end, it may be determined whether embrittlement may have resulted from corrosion. When examining the form of failure for the non-corroded wires, 100% (3/3) of the wires showed signs of ductile failure. This was evidenced by the near perfect necking of the non-corroded strand as seen in Figure 3a. When examining the degree of corrosion for the remaining wires, 68.7% (68/99) of the wires were mildly corroded. Of that, 29.4% (20/68) showed signs of ductile failures, 52.9% (36/68) showed signs of brittle failures, and 17.6% (12/68) showed signs of both ductile and brittle failures. In addition to the mildly corroded wires, the remaining 31.3% (31/99) of corroded wires had moderate levels of corrosion. Of those moderately corroded wires, only 3.2% (1/31) showed signs of ductile failure, while the majority 90.3% (28/31) showed signs of brittle failure, and the remaining 6.5% (2/31) showed signs of both ductile and brittle behavior.

The corrosion observed in most cases was concentrated on the outer surface of the steel strands. After unwinding and observing the individual wires in each strand, it was evident that some of the wires experienced mild to moderate corrosion on the outer surface of the wire, while virtually no corrosion was found on the inside surface of the same wire facing the king strand wire. An example of this is shown in Figure 3-8. In these cases, the king strand wire showed considerably less corrosion than compared to the outer wires.

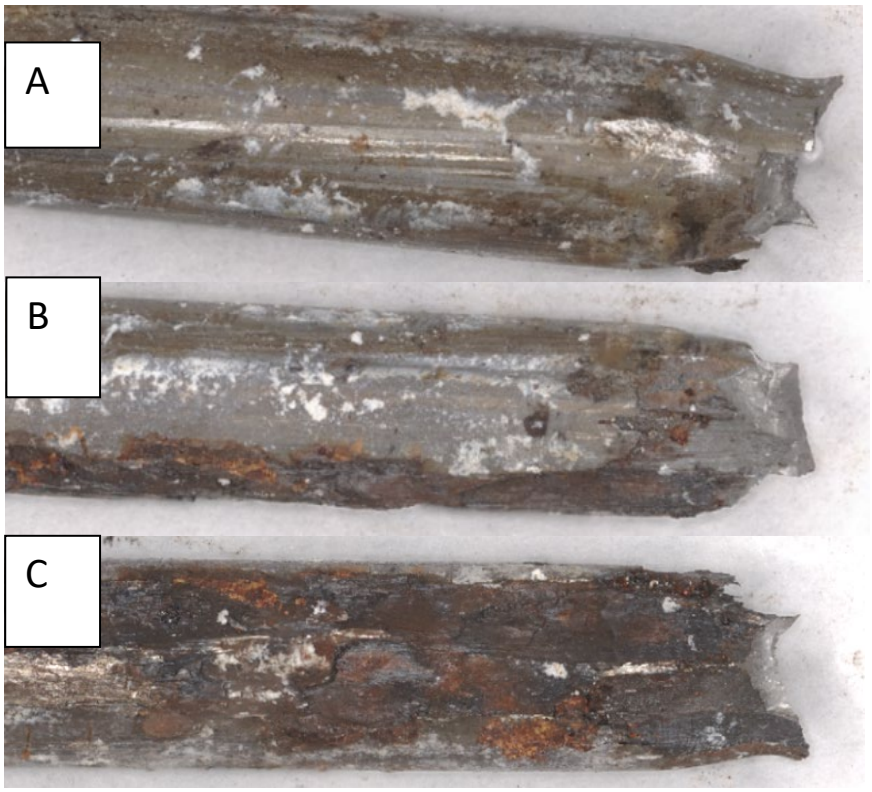

Figure 3-8. Different sides of the same wire showing: (A) inner surface of the wire without corrosion; (B) surface that contacts the neighboring wire with mild corrosion; (C) outer surface of the wire with moderate corrosion.

An example of significant and minimal corrosion pits on the surface of the sandblasted samples can be seen in Figure 3-9. Figure 3-9a shows a moderately corroded wire after removal of the surface corrosion products. Figure 3-9b shows a wire with minimal corrosion pits on the surface. Interestingly, the moderately corroding wires show no sign of necking while the mildly corroded ones show extensive necking.

a)

b)

Figure 3-9. 3D surface images of corroded wire sections near the fracture location; (A) extensive corrosion with brittle fracture; (B) mild corrosion with ductile fracture.

3.3 Reduction in Strength and Hydrogen Content

To estimate the reduction in mechanical performance of the individual wires after the cross-sectional area has been reduced, a relationship between the remaining cross-sectional area of the wire and the fracture strength was used. Equation 3-2 is an empirical relationship developed by Hartt and Lee[45].

$$FS = 19.69 * RCSA - 107.42 \qquad \text{Equation 3-2}$$

In this equation, FS is the residual fracture stress in MPa for the remaining cross-sectional area and RCSA is the reduced cross-sectional area expressed as a percentage[45]. For a wire with no cross-sectional area loss (RCSA = 100%), the typical guaranteed ultimate tensile strength (GUTS) is 1,860 MPa. This equation does not consider corrosion damage morphology and its influence on stress concentrations that would influence residual strength. Additionally, the equation does not consider the possible role of absorbed hydrogen. Estimates made of residual fracture strength using this equation should be considered with caution, however the values obtained may be useful in assessing whether hydrogen may have contributed to premature fracture. For example, if the estimated residual strength greatly exceeded the expected applied load, then it may be likely that hydrogen embrittlement promoted premature fracture.

Jeon et al. also proposed a linear relationship between the residual fracture strength and the residual cross-sectional area but suggested different values for the slope and intercept of the expression based on the 3 different corrosion damage morphologies as described by Figure 3-10 [46]. Based on damage morphology-a which is likely the most indicative to the damage morphology observed, the fracture strength may be expressed as

$$FS = 19.91 * RCSA - 243.8 \qquad \text{Equation 3-3}$$

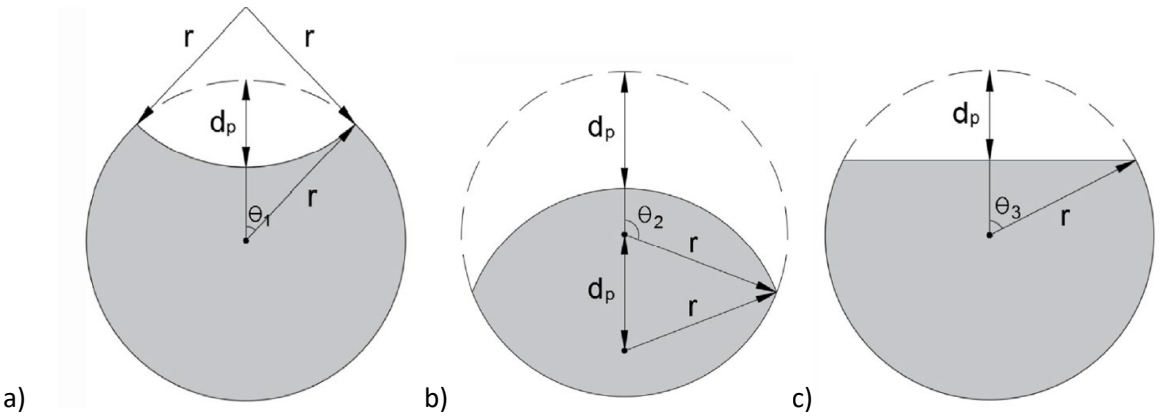

a) b) c)

Figure 3-10. Idealized corrosion damage morphologies proposed by Jeon et al [46].

Estimates of the residual fracture strength based on Equations 3-2 and 3-3 are provided in the last two columns of Table 2. For the outer wires of the strands, the average reduced necking area was 14.8 mm^2; for the king wires, the average reduced necking area was 12.8 mm^2 suggesting that the outer wires may have lost some of their ductility.

Table 2. Quantified reduction of area for selected samples.

Wire	A_0 (mm^2)	A_n (mm^2)	Est. Ductility (%)	A_r (mm^2)	RCSA (%)	FS (2) (MPa)	FS (3) (MPa)
7F	19.6	14.9	24	6.0	40.3	686.9	558.9
15A	19.6	14.8	25	7.4	50.1	868.6	754.1
8A	19.6	14.7	25	8.7	59	1054.1	931.4
5B	19.6	14.8	25	6.0	40.6	691.7	564.9
10A	19.6	14.7	25	11.2	76.1	1390.4	1272.0
6E	19.6	14.7	25	11.2	76.1	1391.3	1271.0
10K	20.4	12.8	37	12.2	95.3	1768.2	1654.4
15K	20.4	12.9	37	12.0	93.3	1729.1	1614.5

According to Hartt[45], the critical fracture stress of the high-strength steel is 63% of the GUTS, approximately 1,172 MPa. If the residual fracture stress is below the critical fracture stress, then the wire is expected to fracture[45]. Based on the estimates of fracture strength, wires 7F, 15A, 8A, and 5B should have fractured according to both Equations 3-2 and 3-3. This indicates that the selected wires would have fractured due to loss of cross-sectional area, regardless of the hydrogen concentration. This interpretation of how the values for the RCSA is calculated lead to reason that the last six selected strands shouldn't have fractured due to solely reduction in cross-sectional area. However, these wires failed in a ductile manner and were likely overloaded following the brittle fractures of neighboring wires. Therefore, the wires that failed in a brittle manner were sufficiently corroded to expect fracture but whether hydrogen absorption influenced the damage rate cannot be determined from the information provided.

The results of the hydrogen testing are shown in Table 3. Based on this table, the four selected samples that were categorized as brittle fractures contained the four highest concentrations of hydrogen and the two samples with a combination of ductile and brittle fracture modes had the next two highest concentrations of absorbed hydrogen. Additionally, the two samples that were categorized as having ductile fractures and the two control samples had the lowest absorbed hydrogen. In a different categorization, wires 7F, 15A, and 5B had the most corrosion and 3 out of the top 4 in terms of the most absorbed hydrogen. For mild corrosion conditions, wires 8A, 10A, and 6E all had intermediate amounts of absorbed hydrogen. Finally, wires 10K, 15K, 10X, and 15X all had virtually no corrosion and had the least amount of absorbed hydrogen. The results reveal a significant correlation between degree of corrosion and hydrogen content suggesting that the absorbed hydrogen present could be a result of the corrosion process. Alternatively, prior existence of absorbed hydrogen could have also facilitated corrosion.

Table 3. Hydrogen content as measured by vacuum hot extraction (ASTM E 146 83).

Sample ID:	Hydrogen Content (ppm)
7F	441
15A	84
8A	75
5B	47
10A	31
6E	6
10K	5
15K	4
10X	3
15X	2

3.4 Discussion on Possible Causes of Failure

Based on information obtained from prior failure analysis reports and our own investigations, several primary causes of failure are possible: (1) the strands may have corroded enough to result in overload and eventual failure; (2) the strands could have absorbed enough hydrogen to become brittle and fracture abruptly; (3) hydrogen absorption combined with corrosion loss could have resulted in failure.

At first glance, the failure of the tendon seems to result from severe corrosion of the strands. This was the conclusion from the ICA and HDR reports from 2017 and 2018, respectively[40, 41]. Their reports detail that upon initial inspection of the failed tendon, they noticed that 5-7 of the 19 total strands were completely rusted through. In addition, they both noted that the section of the tendon where the failure happened was almost completely voided of grout, approximately 80% of the grout was missing[40, 41]. The remaining grout that was present in the failed tendon had a pH ranging from 5-12 as indicated with rainbow pH indicator[40, 41]. A pH of 5 is very low for the typical alkaline grout used for tendons with a pH > 11. With a pH this low, the protective passive film that forms on the steels surface would have been broken down followed by the initiation of corrosion. This inevitable corrosion would likely continue until the cross-section of the strands became too small to support the load, leading to fracture of the strands and subsequently failure of the tendon. However, this process can be accelerated if hydrogen embrittlement is involved.

After the initial reports filed from ICA and HDR were submitted, the University of South Florida received a portion of the failed tendon. Once received, initial inspection of the tendon concurred that there were signs of significant corrosion to the steel strands. In addition to the visual inspection, some samples of the wires both near the fracture location and away from the fracture location were sent to Luvak Inc. for hydrogen content testing. The results from those tests indicated that there were elevated concentrations of hydrogen in the samples taken from near the fracture location compared to the samples that were taken from far away from the fracture location. The additional results presented in this report are in agreement with that. This indicates that hydrogen embrittlement may have played a role in the cause of failure. There are two possible sources of hydrogen within a tendon. Hydrogen could evolve as a cathodic reaction if the steel is polarized sufficiently in the negative direction because of possible galvanic coupling to the galvanized duct. This was shown to be the case during a short period of time directly following placement of the grout and while it is still wet in the work performed by Hartt et al[45].

Another possible source of hydrogen is the hydrolysis of corrosion products as the result of a locally acidic environment produced in an occluded corroding region of the steel strand. The results of our analysis suggest that there may have either been a period of time during the initial grouting process when the combination of higher pumping pressure and older formula of grout used, which did not resist bleeding, allowed for the segregation of the grout mixture to occur. If this is true, the conductive bleed water could have formed a galvanic couple between the galvanized steel duct and the steel strands, promoting hydrogen formation on the cathodically polarized strands until the bleed water was reabsorbed or evaporated. Another possibility is that during the grouting process, a lack of proper grouting could have left some of the steel strands exposed in the high points of the tendon, where the air would have collected. Akiyama et al. evaluated the absorption of hydrogen in atmospherically corroding steel[47]. Under atmospheric conditions in which the strands may reside in a humid environment such as within a voided tendon, a thin moisture layer develops on the strand surface that may have extremely high concentrations of corrosion activators such as chlorides. Corrosion initiated under these conditions usually results in localized pitting in which the local moisture pH can reach as low of 2 or 3. Due to the low pH, the hydrogen

ions can combine to form adsorbed hydrogen molecules which can be absorbed into the steel. Because the failure location of the Wando River Bridge tendon was within a voided duct, this may be the likely failure mode. If hydrogen embrittlement has already occurred, the strands will fracture in a brittle manner before a similarly corroded ductile strand would.

3.5 Summary

Based on the results in Table 2 and Table 3, four of the selected wires that were identified as brittle fractures contained the highest concentration of absorbed hydrogen along with the greatest amount of reduction in cross-sectional area due to corrosion. Two of the selected wires showed signs of a combination of both brittle and ductile behavior and contained moderate amounts of absorbed hydrogen and half of the corrosion compared to the previous four selected wires. The remaining two selected wires, which were identified as ductile fractures, only contained slightly elevated amounts of absorbed hydrogen and minimal surface corrosion. This suggests that there is a correlation between the amount of absorbed hydrogen and the reduction in cross-sectional area due to corrosion, as suggested by recent work from Rudomilova et. al.[48].

Additionally, the qualitative analysis for the degree of pitting corrosion on the outer surface of the wires near the fracture point agrees with the quantitative analysis on the amount of corrosion on the cross-section. The wires identified as having brittle failure consistently had a significant amount of corrosion, both in the cross-section and on the outside of the wire. In contrast, wires identified as having ductile failure had minimal corrosion near the fracture point. Therefore, the failure of the strand may have been localized corrosion of the strands that either contributed to embrittlement or was facilitated by previously absorbed hydrogen. Experiments to determine what conditions within the tendon promote galvanic coupling between the duct and the strands are reported in the next chapter.

4 Quantification of Galvanic Coupling

In this chapter, a series of mock tendons comprising a galvanized steel duct and one centrally placed steel wire were constructed with varying grout conditions. The degree of galvanic coupling between the duct and the steel wire was monitored over time in terms of potential and current density as the different grout conditions hydrated. The results presented reflect the behavior of the first week after casting throughout the life of the specimen. Selected specimens will continue to be monitored for any signs of an increase in galvanic coupling due to the possible depletion of oxygen within the system, which may cause a drop in corrosion potential of the wire. Preliminary simulations of the magnitude of galvanic activity are presented to identify whether oxygen depletion is possible and whether such conditions may promote hydrogen evolution.

Galvanic coupling occurs when two dissimilar metals are connected to each other either through direct physical contact or through electrical connections. For internal post-tensioned tendons, the carbon steel strands, and the galvanized steel ducts are at a minimum electrically grounded to each other, and in some cases, the strands may make physical contact to the ducts at deviation points along the length of the tendon. Because dissimilar metals have different standard electrode potentials, when an electrical connection is made, the resulting mixed potential, known as the corrosion potential, will drive a galvanic couple. If specific conditions are met, microcell or macrocell corrosion will occur. Microcell corrosion occurs when the anode and cathode are on the same surface, typically in a localized area. Macrocell corrosion occurs when the anode and cathode are on separate surfaces that are electrically connected and are in contact with a conductive solution. For this work, the focus was placed on macrocell corrosion driven by the strand-duct galvanic couple.

For internal post-tensioned tendon system, the macrocell corrosion reactions that are driven by the strand-duct galvanic couple are influenced by several factors. First, the difference between the standard electrical potential and the corrosion potential must be sufficient to drive electrons from the anode to the cathode. For carbon steel and galvanized steel, the difference between the zinc standard electrical potential and iron standard electrical potential is sufficient to produce a mixed corrosion potential that will polarize the galvanized steel duct anodically and the carbon steel strands cathodically. The next factor that influences macrocell corrosion is the conductivity of the solution in contact with the anode and cathodes. For post-tensioned tendons, the grout that is pumped into the tendon during casting acts as this conductive solution. Typically, the grout is most conductive when it is first mixed and pumped into the tendons during casting. As the grout cures and hydrates over time, the conductivity decreases as the resistivity increases. Therefore, most galvanic activity will occur while the grout is conductive within the first few days after casting. During this time, the corrosion current is ohmic limited based on the corrosion potential and the resistivity of the grout. In extreme cases, mild rainwater or aggressive marine water may contaminate the grout mixture or may be introduced into the tendons through improper sealing at expansion joints or vent pipes. In these cases, the increased conductivity of the mild or aggressive water can facilitate further galvanic corrosion. Finally, the exposed surface area of the inside of the duct and the outside of the strands are factors in determining the corrosion current density.

4.1 Experimental Methods

The experiments performed for this report were designed to test different grout conditions and quantify any galvanic coupling that may be formed during casting. To achieve this, several tendon segments were cast using ASTM A53 seamless hot-dipped galvanized steel pipe segments cut into 6-in lengths, straight center king wire strands from ASTM A416 7-wire uncoated steel strands cut into 10-in lengths, and EUCO Cable Grout PTX mixed with varying amounts of water (w/c = 0.28, 0.38, 0.5, and 0.28 with 3.5% NaCl by weight of water). The water to cement ratio recommended by the grout manufacturer ranges from 0.25-0.28. By varying the amount of water used and including a chloride-contaminated condition, the effects of porosity and grout resistivity can be assessed. For the recommended condition, two tendons with a water to cement ratio of 0.28 were cast. The next batch of four tendons had double the manufacturers recommended water to cement ration of 0.5; similar to the water to cement ratio of 0.47 used for the concrete piles investigated by Hartt and Suarez [11]. The last batch of three tendons that were cast using a water to cement ratio in between the first two batches of 0.38. In addition, a full-length graphite counter electrode and 2-inch mixed metal oxide reference electrode were embedded to perform electrochemical impedance spectroscopy measurements during curing. Table 4 shows when each batch of tendons were cast. Figure 4-1 shows the schematic of the cast tendons.

Table 4. Name, water-to-cement ratio, and date of tendon batch castings.

Tendon Batch Name	Water to Cement Ratio	Age (Days)	Number of Tendons
Good Grout	0.28	299	2
Very Soft Grout	0.50	270	4
Semisoft Grout	0.38	194	3
NaCl Grout	0.28	135	6

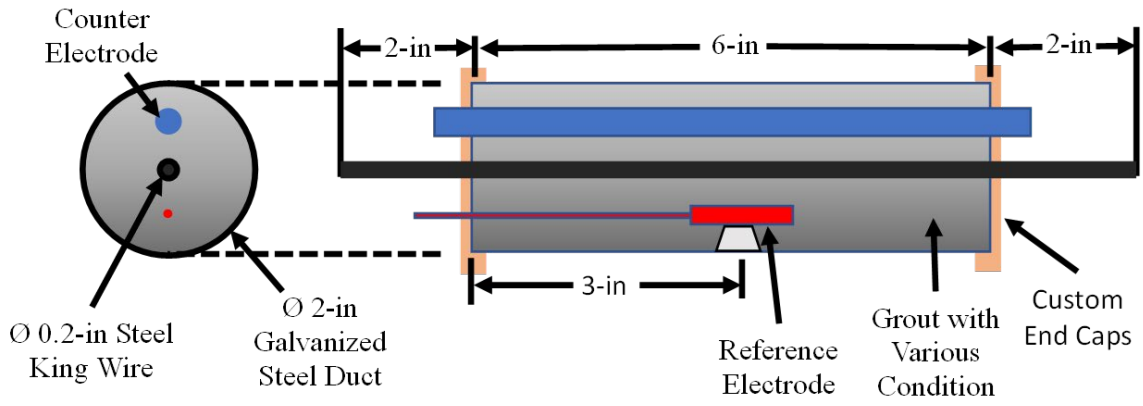

Figure 4-1. Schematic of cast internal tendon segments.

The unstressed strand and electrodes were held in place during casting using two 3D printed endcaps, one solid and one with ports to allow for the addition of the grout. The tendons were cast vertically, and the lower end cap was sealed using a two-part epoxy that is stable in high pH environments to prevent bleed water from discharging out of the tendons. During casting, the tendons were tapped on the side with a rubber mallet and the workable grout was rodded to remove any air bubbles. Directly following

casting, a zero-resistance ammeter was used to monitor the cell potential and galvanic current density over an approximately 1-week period. The zero-resistance ammeter operates by imposing a current density that maintains a zero-potential difference between the two connected metals, which in this case are the galvanized steel duct and the steel wire. In this way, the amount of polarization applied to each material is monitored. The reported potential is equal to both the interfacial potential between the duct and the grout and the interfacial potential between the steel wire and the grout, which is reported in reference to the reference electrode material. The current required to maintain a zero-potential difference between the two metals is also monitored and represents the galvanic current. Leftover grout from each mixture was poured into plastic 2-inch-diameter 4-inch-tall plastic molds, each with four stainless steel screws threaded into the side of the containers. Periodic resistance measurements were performed on these cylinders to determine the resistivity of the different grout mixtures as they cured over time. Periodic electrochemical impedance spectroscopy (EIS) measurements were also performed on the tendon segments. EIS is a nondestructive electrochemical testing technique in which a small sinusoidal perturbation potential is applied to a working electrode across a wide range of frequencies. During this test, the current between the working and a counter electrode is measured while the potential is recorded in reference to an embedded reference electrode. Due to the wide frequency range of EIS testing, information about electrochemical reactions can be obtained. For these tests, the steel strand was the working electrode, and the counter electrode was an embedded graphite rod. As the grout cured, the interfacial capacitance between the steel strand and the different grout mixtures was measured along with any corrosion reactions that may have been occurring.

In addition to the different grout mixtures, two pairs of tendons were filled with a mild water solution (100 ppm Cl^- and 200 ppm SO_4^{-2}) and an aggressive water solution (3.5% NaCl) instead of grout. These tendons were representative of a worst-case scenario where the tendon is void of grout and rain or sea water enters the tendon, filling the void from duct to strand. While voids alone within the tendon duct that may not be filled with solution were previously shown to result in hydrogen absorption, the mechanism that produces the hydrogen in that case cannot be due to galvanic coupling and therefore was not included in this work. For these experiments, no counter electrode was used, and a saturated calomel electrode replaced the mixed metal oxide reference electrode. After the solutions were poured into the tendons, galvanic potential and current were recorded.

Additionally, separate measurements were performed to study cathodic reaction kinetics of the prestressing steel. Figure 4-2 shows a schematic of the cathodic kinetic experiment. This experiment was set up using a sealed electrochemical test cell filled with a saturated calcium hydroxide solution to represent the high alkaline environment of the grout. The pH of the saturated calcium hydroxide was 12.5-13. Immersed in this solution was a single king wire strand of the same batch, type, and size used for the previous tendon experiments. This single strand was covered in epoxy to limit the exposed surface area to a finite amount. Once the exposed surface area was immersed in the solution, an open circuit potential was measured, followed by a potentiodynamic test, followed by another open circuit potential. These tests were run using the strand as the electrode, a piece of stainless-steel mesh as the counter electrode, and a standard calomel electrode (SCE) as the reference electrode. Due to the destructive nature of the potentiodynamic test, each strand was only used for one test. These tests were repeated using different solutions that were either aerated or deaerated to determine how oxygen depletion influences the cathodic kinetics of the steel.

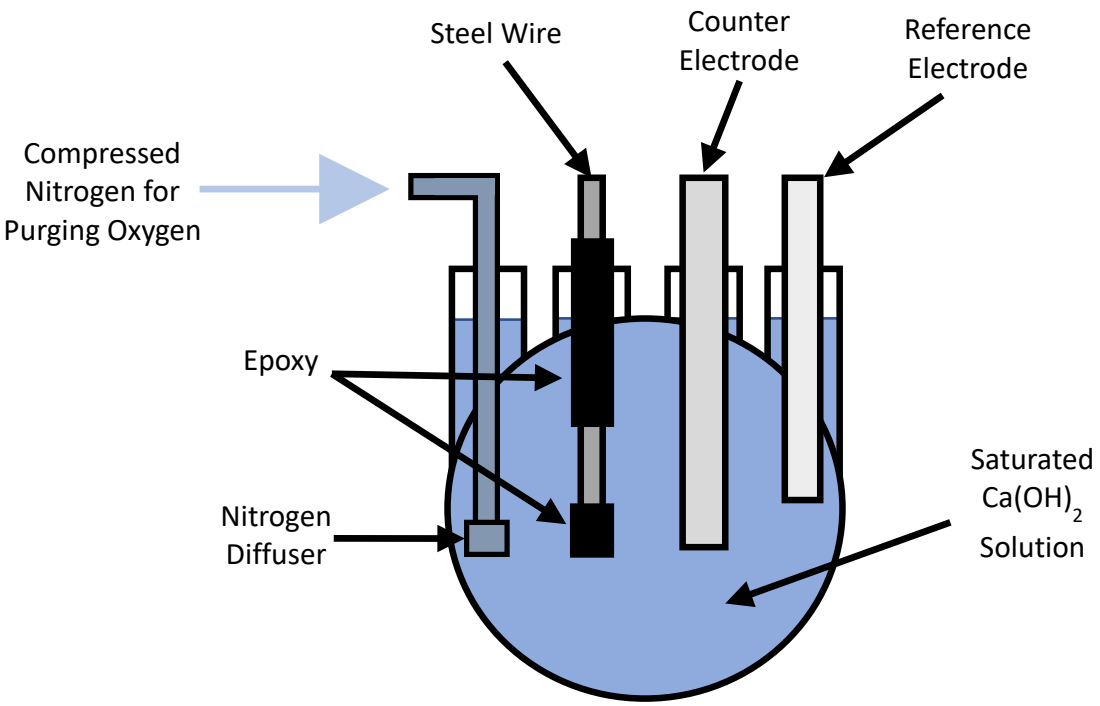

Figure 4-2. Schematic of cathodic kinetic experiment.

In conjunction with the tendon experiments and cathodic kinetic experiments, a finite element model was constructed to recreate the different tendon grout scenarios tested in the tendon experiments and to examine the possibility of oxygen depletion within the tendons.

4.2 Experimental Results

The results of the galvanic coupling experiments are shown below for the first week following casting. Figures 4-3 and 4-4 respectfully show the potential of the steel wire and the galvanic current density of these three batches plotted as a function of time in log-scale. For ease of interpretation of the general trends, all the results of each tendon were grouped by their water to cement ratio and set to the same color. Since zinc has a more negative corrosion potential than the prestressing steel, the galvanized duct polarizes the prestressing steel to more negative values than its corrosion potential while the duct is polarized to more positive (anodic) potentials than its corrosion potential. The cell potential reported is the amount of polarization applied to each material and should be a value between the two corrosion potentials of each material. The cell resistance or the resistance between the duct and the steel wire in some cases controls the amount of galvanic coupling possible. As the resistance between the two materials decreases, the galvanic couple strengthens, and the steel wire is increasing cathodically polarized. If the steel is overly polarized to more negative values, hydrogen evolution will occur which may lead to embrittlement of the prestressing steel. The galvanic current density is the total current scaled by the surface area of the strand. Therefore, the ideal scenario is for a minimal galvanic couple to form with a weak galvanic potential drop and low galvanic current density.

According to the results, tendons cast with the recommended water to cement ratio resulted in the most positive cell potential indicating minimal galvanic activity. The tendons cast with intermediate water to cement ratio grout yielded cell potentials (< -900 mV_{SCE}) that may suggest hydrogen evolution is likely.

The tendons cast with the high water to cement ratio resulted in cell potentials that were well below the -900 mV_{SCE} threshold [8] and multiple current density peaks.

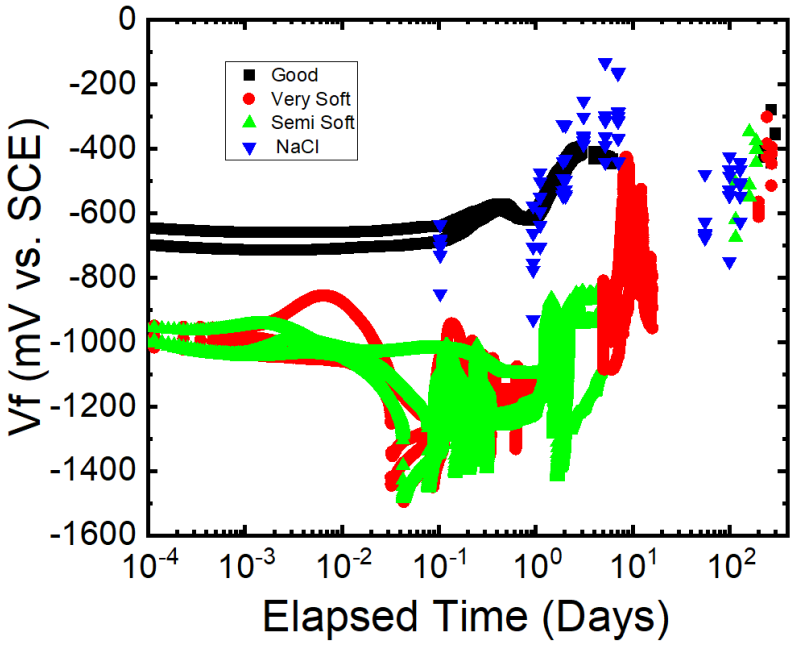

Figure 4-3. Galvanic potential as a function of time in log-scale with grout water-to-cement ratio as a parameter.

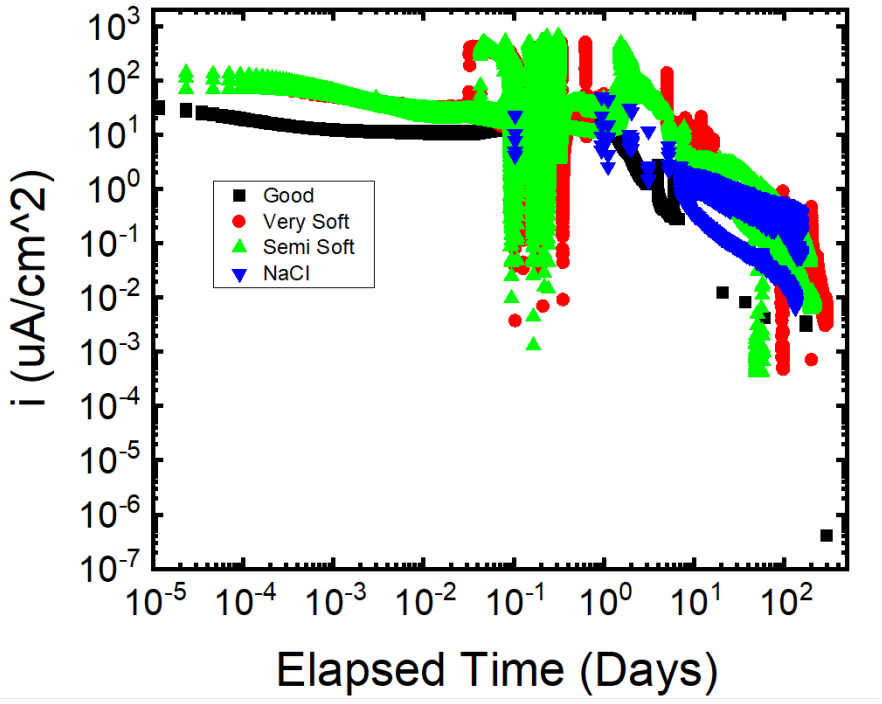

Figure 4-4. Galvanic current density in log-scale as a function of time in log-scale with grout water-to-cement ratio as a parameter.

To monitor the curing rates of the different grout mixtures, samples from each of the grout batches were collected and measured periodically to determine the grout resistivity. Figure 4-5 shows the resistivities as a function of time considering a geometric conversion factor according to the dimensions of the cylindrical grout samples and according to the formulation presented in Morris et. Al. [12].

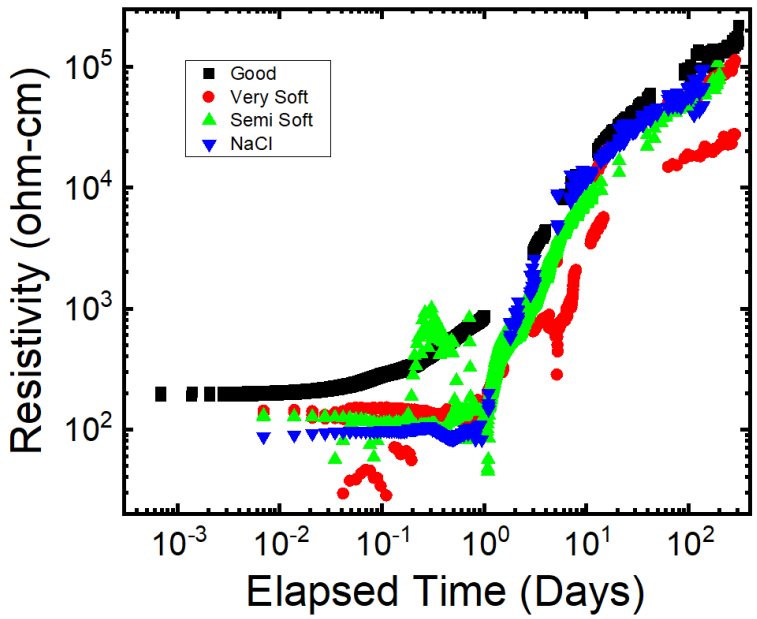

Figure 4-5. Grout resistivity in log-scale as a function of time in log-scale with grout water-to-cement ratio as a parameter.

Based on this data, the resistivity of each of the grout mixtures remained low initially after casting, while the grout was still workable, and began to increase after the first day regardless of the water to cement ratio. As expected, the increased water content in the higher water to cement ratio grouts increased the conductivity of the initial mixture and therefore decreased the resistivity of the initial mixtures. Because of this lower initial grout resistivity for the higher water to cement ratio grouts, any galvanic polarization of the steel strand would be strengthened. Additionally, the higher conductivity grout allows for increased galvanic current to flow in between the strand and the duct.

The cell potential and galvanic current density of the solution filled tendons are shown in figures 4-6 and 4-7, respectively. The first batch of three tendons were filled with a mild water solution followed by two batches of three tendons filled with an aggressive water solution. For ease of interpretation of the general trends, all the tendons that were filled with mild water were colored the same and all the tendons that were filled with aggressive water were colored the same. In these figures, it is shown that immediately upon adding either of the two solutions to the voided tendons, all the potentials drop below the -900 mV_{SCE} threshold for the hydrogen evolution reaction to occur [8]. This is followed by an increase in current density that maintains throughout the experiments. It is important to note that the current densities initially peak over 100 $\mu A/cm^2$ and remain above 10 $\mu A/cm^2$ after a week of exposure in the mild water solution and above 20 $\mu A/cm^2$ for the aggressive solution. To understand the significance of these current densities and to better understand the cathodic kinetics of the steel strands, cathodic polarization

experiments were performed on steel strands in a saturated calcium hydroxide solution which is often used to simulate the grout pore solution. Figure 4-8 expresses the measured current density as a function of the applied potential.

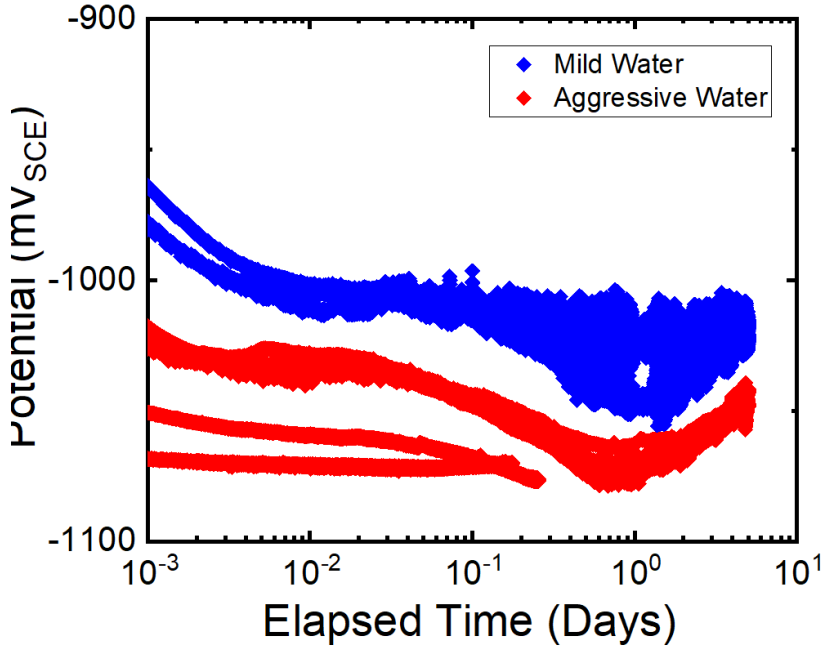

Figure 4-6. Galvanic potential of tendons as a function of time in log-scale with mild or aggressive water solution as a parameter.

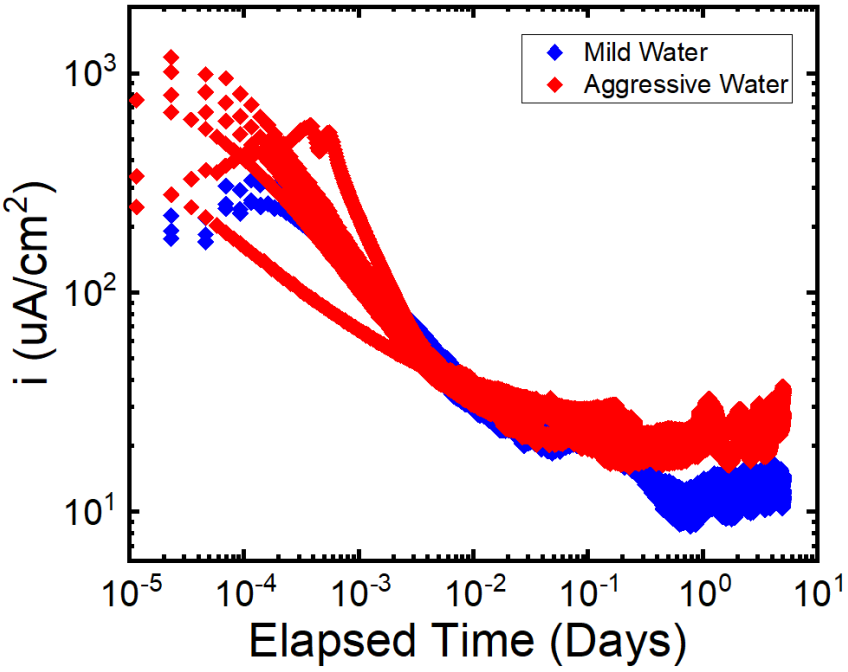

Figure 4-7. Galvanic current density in log-scale as a function of time in log-scale with mild or aggressive water solution as a parameter.

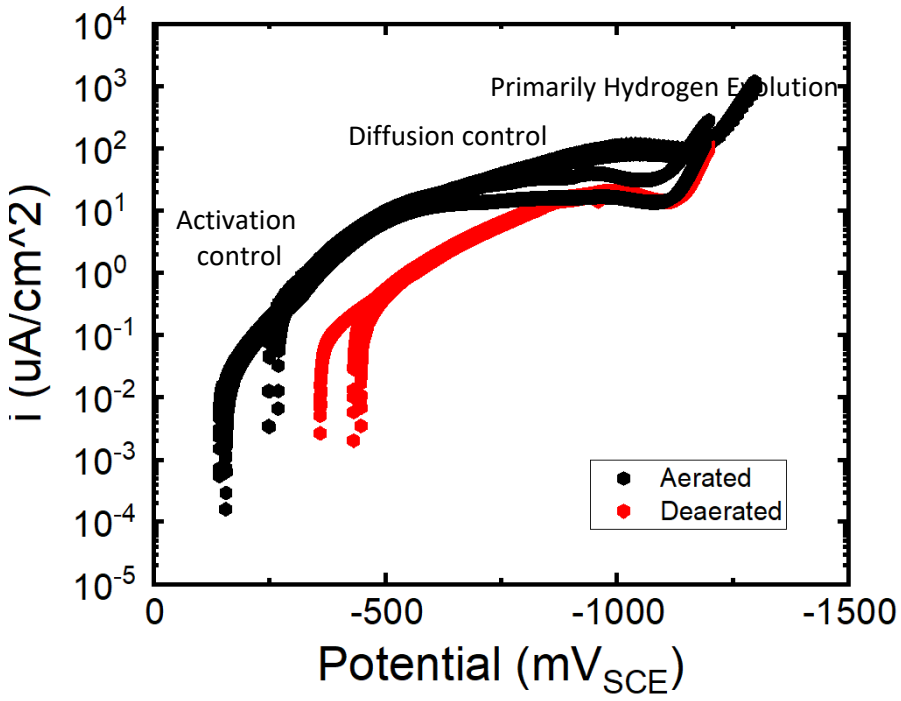

Figure 4-8. Steel strand potential as a function of current density in log-scale with aeration as a parameter.

According to the data, when the strand potential is near the open circuit potential, the current density is minimal. As the strand becomes cathodically polarized in the negative potential direction, the oxygen reduction reaction is activation controlled as seen by the visually linear portion of the curve which is due to an exponential dependence of potential on the current density. This reaction continues until the bulk of the dissolved oxygen is consumed resulting in a cathodic current that is now limited by the diffusion of oxygen from the bulk solution to the surface of the strand. This limitation can be seen as the horizontal section of the curves in the 10-100 μA/cm^2 range with varying cathodic potentials. As the strand potential is cathodically driven lower, the rate of the hydrogen evolution reaction exceeds the diffusion limited current density associated with oxygen reduction as indicated by a sudden increase in current density.

Based on Figure 4-6 to Figure 4-8, the elevated current densities of the voided tendons filled with mild and aggressive water show that the hydrogen evolution reaction was likely occurring throughout the duration of those experiments. Further evidence of the hydrogen evolution reaction can be seen in Figure 4-9. This figure shows a photo of one of the solution-filled mock tendons at the end of the experiment where small bubbles were visible at the steel solution interface likely resulting from their formation due to hydrogen evolution at the steel strand surface.

Figure 4-9. A photo of a galvanized steel duct filled with an aggressive water solution after one week of exposure showing hydrogen bubbles forming on the surface of the steel.

Figure 4-10 shows the the measured corrosion potential of the steel wire as a function of time with the grout condition as a parameter. The most negative value (~-1.18 V_{SCE}) was measured immediately after casting of the chloride-contaminated grout condition. After approximately 100 days the corrosion potential reached values between -0.6 and -0.3 V_{SCE}. A similar behavior was observed for the very soft grout condition with the most negative potential measured of -1.1 V_{SCE} and reaching values between -0.4 and -0.25 V_{SCE} after 250 days of exposure.

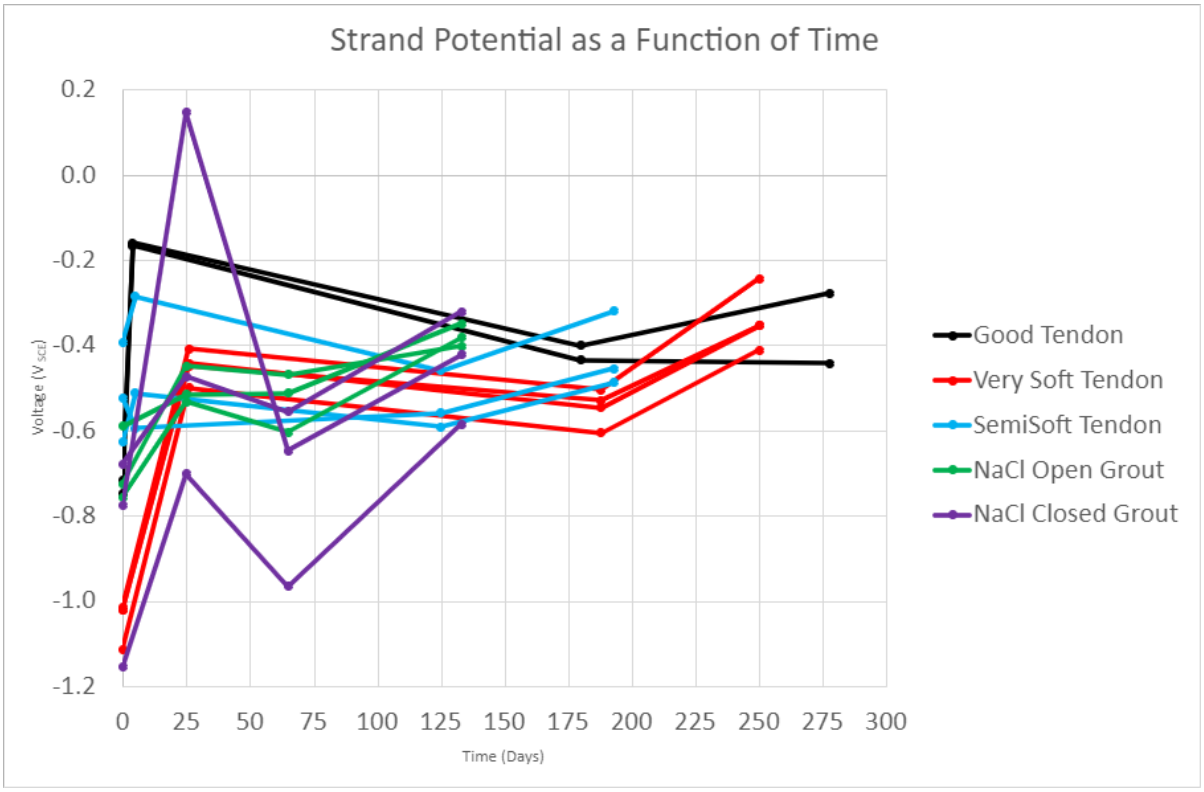

Figure 4-10. Strand corrosion potential vs. SCE over time for each grout condition.

The electrochemical impedance spectroscopy results are shown in Figure 4-11 for each grout condition with exposure time as a parameter. The greatest impedance was measured on the good grout tendons suggesting little corrosion activity. These results were used to calculate the corrosion current density as a function of time for each grout condition which will be incorporated into the simulations presented in section 4.3.

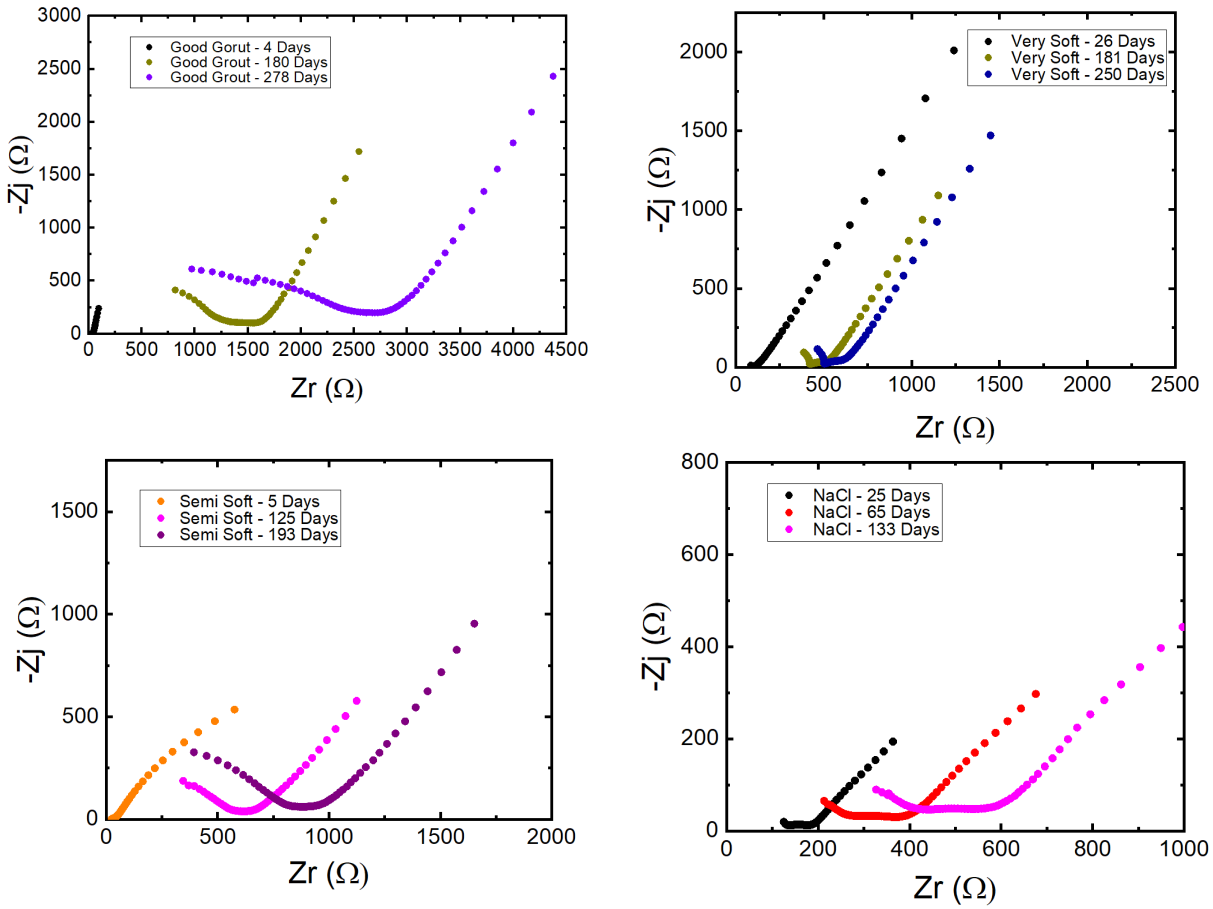

Figure 4-11. Steel wire impedance for each grout condition at beginning and end of exposure.

4.3 Galvanic Coupling Simulations

The level of galvanic coupling measured through the single wire mock tendon experiments are specific to the geometry utilized. However, the results provide the necessary parameter values to predict the level of galvanic coupling considering typical tendon geometries that include multiple 7-wire prestressing steel strands. The experimental results obtained were incorporated into a finite element model considering typical tendon geometries to simulate the galvanic coupling between the galvanized steel duct and the prestressing strands provided the grout conductivity that was measured for the various grout conditions.

4.3.1 Model Description

Initial simulations were performed of the mock tendon geometry for confirmation that the model was able to accurately predict galvanic activity considering the measured kinetic parameters. The model geometry is described by the schematic shown in Figure 4-10.

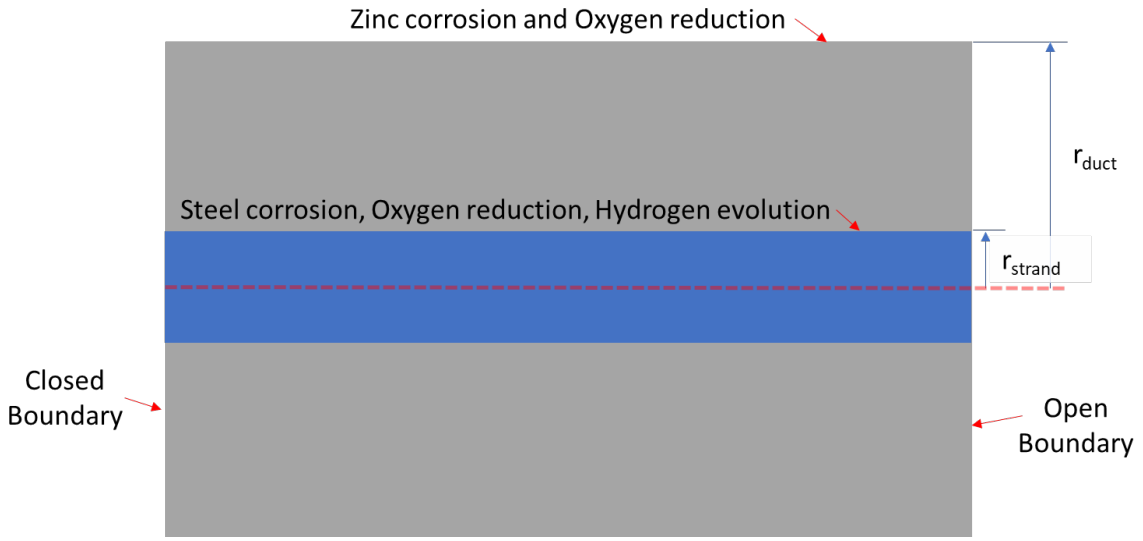

Figure 4-12. Schematic of simple model geometry with descriptive boundary conditions.

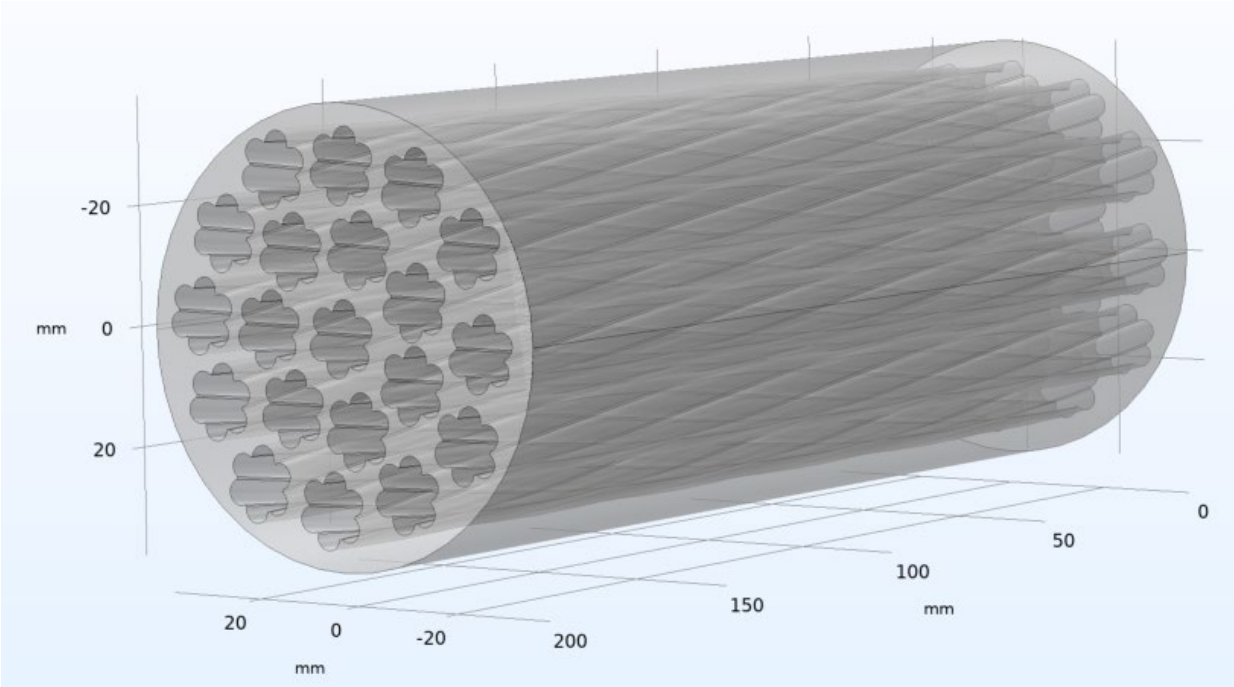

Figure 4-13. Schematic of idealized tendon model considering true strand geometry.

The model is used to simulate the potential distribution throughout the grout provided the corrosion potential and corrosion current densities of both the strands and the duct based on the experimentally measured values. Hydrogen evolution is incorporated into the kinetic expression for the steel boundary. Laplace's equation is assumed to govern the potential distributions where

$$\nabla^2 \varphi = 0 \qquad \text{Equation 4-1}$$

The kinetic expressions considering both anodic and cathodic activity of each material are assumed to follow Tafel kinetics. Iron corrosion, oxygen reduction, and hydrogen evolution were the reaction considered at the steel strand surface according to a current density expressed as

$$i_{\text{steel}} = i_{1,\text{corr}} \left[\exp\left(\left(V - \varphi - E_{1,\text{corr}}\right) \frac{2.303}{B_{1,\text{a}}} \right) - \exp\left(-\left(V - \varphi - E_{1,\text{corr}}\right) \frac{2.303}{B_{1,\text{c}}} \right) \right] + i_{\text{c,H}}$$

where $i_{c,H}$ is expressed as

$$i_{c,H} = -i_{0,H} \exp\left(-\left(Vm - \varphi - E_{0,H}\right) \frac{2.303}{B_H} \right)$$

A similar expression was used to describe the kinetics at the galvanized steel duct as

$$i_{\text{duct}} = i_{2,\text{corr}} \left[\exp\left(\left(V - \varphi - E_{2,\text{corr}}\right) \frac{2.303}{B_{2,\text{a}}} \right) - \exp\left(-\left(V - \varphi - E_{2,\text{corr}}\right) \frac{2.303}{B_{2,\text{c}}} \right) \right]$$

The parameters were set to values either that were either measured or from the literature as described in Table 5. The corrosion potentials of each material were set to values obtained from literature that reflect the natural potentials of the material when exposed to the grout.

Table 5. Model input paramters

Parameter	Value	Description
V	0[V_{SCE}]	Applied potential
E1,corr	-.8[V_{SCE}]	Measured steel corrosion potential
E2,corr	-1.2[V_{SCE}]	Literature duct corrosion potential
i1,corr	2.63e-6[A/cm^2]	Measured steel corrosion current density
i2,corr	9e-6[A/cm^2]	Literature duct corrosion current density
B1,a	0.4[V/dec]	Steel anodic Tafel parameter
B1,c	0.18[V/dec]	Steel cathodic Tafel parameter
B2,a	0.06[V/dec]	Duct anodic Tafel parameter
B2,c	0.06[V/dec]	Duct cathodic Tafel parameter
E0H	-1[V_{SCE}]	Abstracted hydrogen potential from measurement
i0H	0.11[µA/cm^2]	Abstracted hydrogen exchange current density from measurement
BH	.18[V]	Measured hydrogen anodic cathodic parameter
k	1[S/m]	Measured grout conductivity

4.3.2 Mock Tendon Simulation Results

The mock tendon simulations were used to ensure that the model accurately reflected the experimental results of the same geometry which allows for application of the model to other geometries. It was assumed that oxygen is abundantly available and only becomes depleted near the cathode surface resulting in a cathodic diffusion limited current density of 100 μA/cm^2 as obtained from the data in Figure 4-8. The kinetic parameter values adopted were the worst-case scenario in which the values were obtained from the beginning of the exposure duration in which the highest level of galvanic activity was measured. The simulations were then performed with the grout resistivity as a parameter for values ranging from 10^{-3} to 10^{6} Ωm. This resistivity range greatly exceeds the measured values but was used to show the limitations of galvanic coupling at low and high resistivity limits.

Figure 4-15 shows the calculated galvanic current density as a function of grout resistivity with horizontal lines that reflect the measured and calculated ranges. The calculated maximum galvanic current density is slightly lower than the measured; however, the calculated range is within the measured range. The large difference between the measured and calculated minimum current density is likely the result of using the early exposure data while the measured minimum current density was obtained at later exposure times after the corrosion potentials of the steel and duct became much more positive. Nevertheless, the comparison between the simulated and measured data suggests the model can estimate the level of galvanic activity and may be used to estimate the galvanic activity that may be achieved in typical tendon geometries.

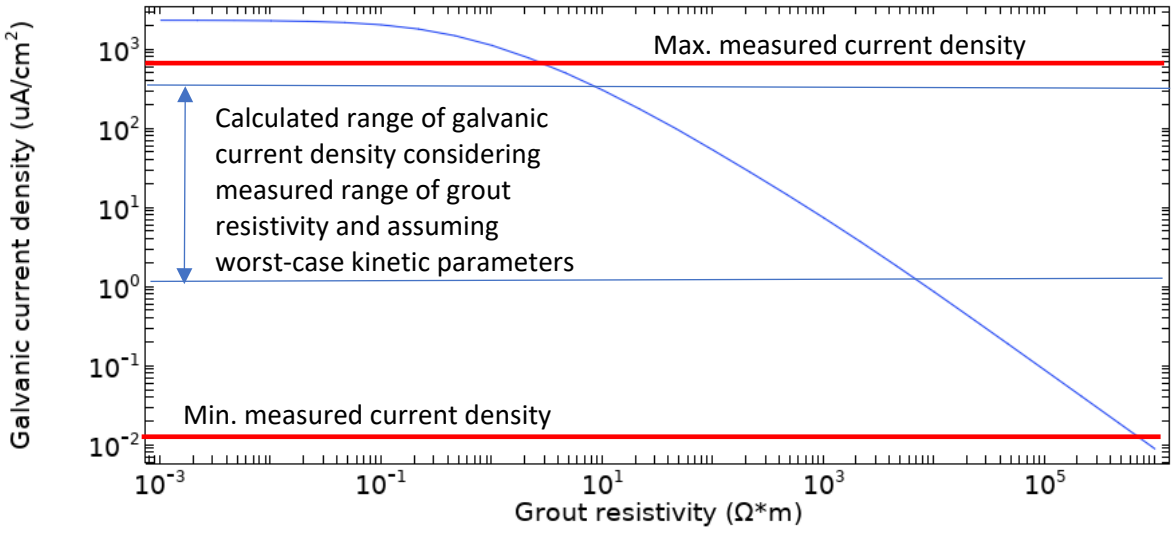

Figure 4-14. Galvanic current density as a function of grout resistivity. The red horizontal lines represent the limits of current density measured in the single wire mock tendon experiments. The blue horizontal lines are the corresponding calculated values.

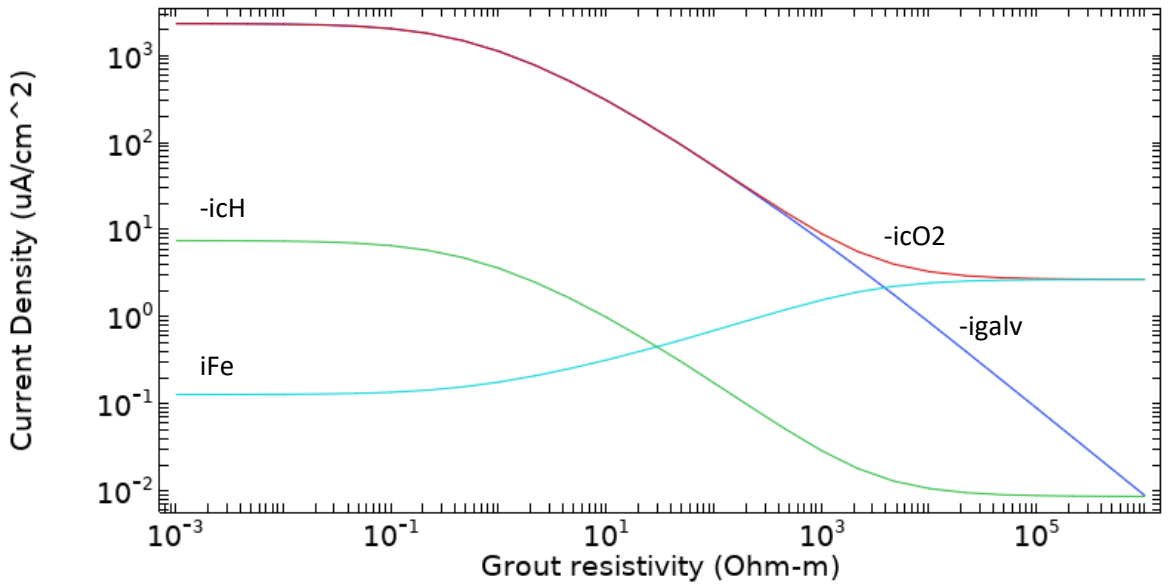

Figure 4-15 Current density as a function of grout resistivity for the total galvanic current density and its anodic and cathodic components for the mock tendon geometry.

Additionally, the model may be used to estimate the portion of the cathodic current density that reflects hydrogen evolution versus oxygen reduction. Figure 4-15 shows the current density as a function of grout resistivity in log-log scale distinguishing between anodic and cathodic contributions of the total galvanic current density. At the lowest resistivity value, the current density associated with the hydrogen evolution reaction is ~7 µA/cm^2 corresponding to the production of ~3x10^{-6} mole/day/cm^2 of hydrogen. At the highest resistivity, the hydrogen evolution current density is ~9x10^{-3} µA/cm^2. This result suggests that even for the worst kinetic conditions and if the grout resistivity to high enough, there will be very limited hydrogen production.

4.3.3 Typical Tendon Simulation Results

The simulated results are shown in Figure 4-16 for the idealized tendon geometry shown in Figure 4-13 in which 20 strands are distributed within a 3-inch-diameter duct. The higher number of strands causes distribution of the total galvanic current over the entire steel strand surface resulting in a lower current density but the proximity of the strands to the duct will increase the galvanic coupling. For the typical tendon geometry at the lowest simulated grout resistivity, a maximum hydrogen evolution current density of ~2.5 µA/cm^2 was calculated which almost a third of the amount calculated for the single wire geometry. Therefore, the experiments performed for the single wire geometry would result in more galvanic coupling than an actual tendon with multiple strands.

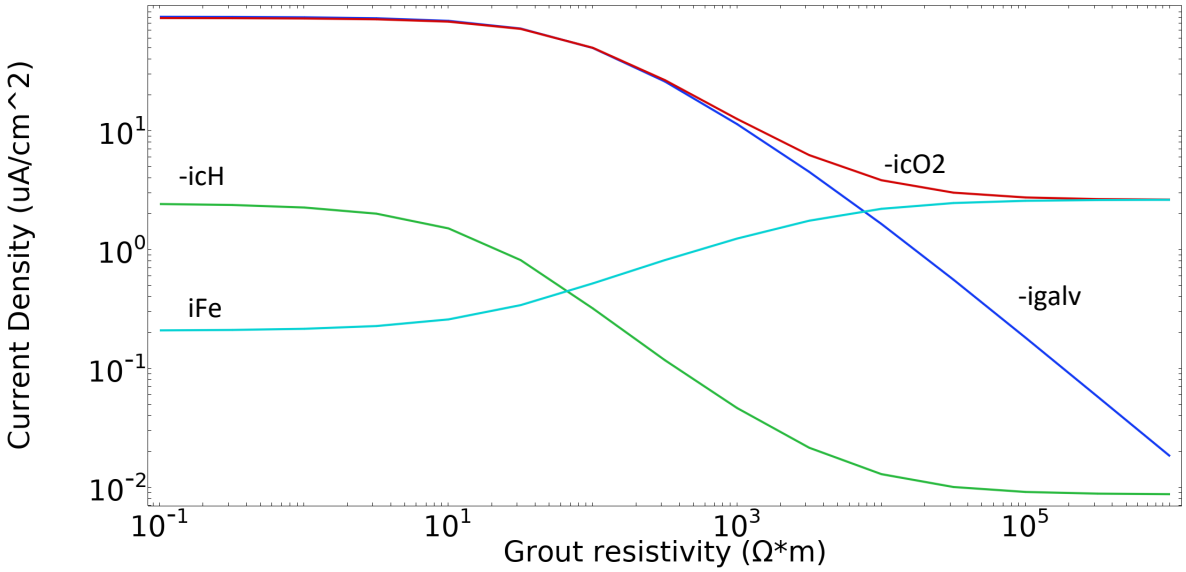

Figure 4-16 Current density as a function of grout resistivity for the total galvanic current density and its anodic and cathodic components for an idealized tendon geometry.

4.4 Summary

In this chapter, the amount of galvanic coupling achievable for several grout conditions was assessed by experiments and simulations. The experiments provided galvanic current density, galvanic cell potential, and grout resistivity as a function of time for each grout condition. Additionally periodic measurements of the steel wire impedance and corrosion potential provided data that could be incorporated into the galvanic coupling simulations considering the mock tendon and an idealized tendon geometry.

The experimental results suggests that the level of galvanic coupling achievable strongly dependent on the resistivity of the grout. Once the grout resistivity begins to increase due to the setting and formation of the solid grout matrix, the galvanic current decreases substantially and the cell potential becomes more positive than the expected cutoff for hydrogen evolution even in the very soft conditions. According to the results of the specific grout tested in this work, if the grout is mixed to the manufacturer's recommendations there is minimal chance for hydrogen evolution even during the grout setting period. If for some reason additional water is inadvertently added during the mixing process, hydrogen evolution may occur within the initial setting period (~1 day) of the grout until the resistivity increases to substantial values (~10 Ωm) to prevent it. Another concern is if voids are present within the ducts that could become filled with water. Under these conditions the experimental results show that hydrogen evolution would be a major concern under these conditions for both mild and aggressive waters.

The simulations were used to quantify the level of galvanic activity that can be expected for typical tendon geometries being that it would have been difficult to measure this accurately in the lab. The simulations considered a 20 strand 3-inch-diameter tendon incorporating the measured kinetic parameters. The results suggest that the maximum achievable rate of hydrogen evolution is approximately 1/3 of that of the mock tendon geometry assuming that oxygen is not depleted due to of the cathodic activity at the steel strands.

5 Implications to Mechanical Properties

In this chapter, results of mock tendons autopsies are presented which were performed to determine the extent of any grouting deficiencies caused by the mixing proportions and determine how the mechanical properties of the steel wires may have been altered due to hydrogen absorption as a result of galvanic coupling. Hydrogen content analysis of the steel wires was performed by Luvak Inc. in Boylston, MA. Autopsied steel wires were subjected to reverse-bend testing to qualitatively assess the hydrogen's influence on ductility. Due to time constraints, slow strain rate testing to obtain full stress-strain responses could not be performed in the allotted time. Additional steel wires were charged with hydrogen to similar levels to total charge passed as the mock tendons to provide a comparison of ductility after charging in various solutions. Reduction in fracture initiation stress was estimated according to empirical formulas for prestressing steel presented in the literature. A discussion is included to describe the limitations of the study and provide context to the results.

5.1 Experimental Methods

The tendons were individually autopsied starting with one from each batch of grout condition including the various water to cement ratios and chloride-contaminated grout case. To remove the galvanized steel duct, an angle grinder was used to cut along the length of the tendon on two sides. Once the duct was cut into two distinct halves, an angled chisel was inserted into the cut and gently tapped with a hammer. The chisel was repositioned along each cut with taps given every inch until the grout was cracked from one side to another. Once the tapping was complete the tendon could be separated into two nearly equal halves, exposing the central wire, and exposing the reference and counter electrodes. Immediately after separating the tendons, a phenolphthalein pH indicator solution was sprayed onto each half to visually alkalinity variations. The two tendon halves were imaged, and the prestressing steel wire was removed and inspected for any visual signs of corrosion or embrittlement. Lastly, the remaining grout was removed from the duct to inspect the grout-duct interface looking for any discolorations or corrosion products.

Once the wires were removed from the tendons during autopsy, they were prepared for hydrogen content testing by Luvak Laboratories using hot vacuum extraction. To expedite testing times, specific locations on each wire were chosen for testing based on each autopsy result. For the good grout (w/c = 0.28) tendon, one sample was selected in the middle of the tendon near the reference electrode. For the very soft grout (w/c = 0.50) tendon, two samples were selected, one in the upper portion and one in the lower portion of the tendon. For the semisoft grout (w/c = 0.38) tendon, two samples were selected, one in the upper portion and one in the central portion of the tendon. For the NaCl contaminated grout (w/c = 0.28) tendon, one sample was selected in the middle of the tendon near the reference electrode. As a control, one sample was chosen from the original wire that was used to cast each tendon; this wire strand was not exposed to any grout mixtures but was in the lab near the cast tendons. Each wire sample was cut to a 1-inch nominal length using a slow speed saw cutting at approximately 350 rpm for an average of nine minutes pet cut. For cooling purposes, an anti-corrosion cutting fluid was used during each cut. Once the samples were cut to length, they were glass-bead blasted to remove any surface contaminants and thoroughly rinsed with ethanol to remove any remaining residues. After rinsing, the samples were dried, placed into individually sealed plastic bags, and shipped to Luvak Laboratories.

The pH of the grout was measured at locations adjacent to the wire segments that were evaluated for hydrogen content. The pH was determined using a modified version of the hot water extraction method called the espresso method. For this method, 10 grams of the desired grout were collected and ground using a mortar and pestle. This sample was placed in a Büchner flask and funnel using a number 41 filter paper element. The flask was connected to a vacuum pump while approximately 300 ml of boiling deionized water was added slowly to the grout sample. The resulting solution was transferred to a 500 ml volumetric flask, capped, and left to cool overnight. After cooling, the solution was brought to 500 ml by adding deionized water and mixed thoroughly. Lastly, a 30-ml sample was tested using a digital pH meter. The sample was measured three times, with the pH probe being rinsed with deionized water in between each measurement. Inductively coupled plasma-optical emission spectrometry (ICP-OES) was performed to determine the concentration of specific elements (potassium (K), sodium (Na), calcium (Ca)) and ion chromatography was performed to obtained ionic concentrations of chloride (Cl^-), sulfate (SO_4^{2-}).

The accumulated charge passed due to galvanic coupling between the single king wire and the galvanized steel duct within the cast tendons during their lifespan was calculated. The recorded current density data were integrated and multiplied by the surface area of the wire to calculate total charge for each cast tendon. The average calculated accumulated charge for each grout condition was used to reproduce the approximate hydrogen charging on new single wire to expedite testing of the mechanical properties. New single wires were charged using a hydrogen charging solution composed of 125 ml of sulfuric acid (H_2SO_4), 875 ml of deionized water, and 0.5 grams of antimony trioxide (Sb_2O_3), which acts as a recombination poison. Hydrogen charging was also performed in a saturated calcium hydroxide ($Ca(OH)_2$) solution used to simulate the grout pore water. A hydrogen charging station was assembled using a 500-ml high-density polyethylene (HDPE) container with a hole in the lid and on the bottom just large enough to allow the wire to be inserted. Once the wire was inserted into the container, a small amount of JB Kwik was used to seal the bottom of the container to prevent leaks. Two additional holes were made in the lid to house the graphite electrode and to act as a vent hole. The graphite electrode was held in place with JB Kwik on top of the lid. A lab stand was used to hold the HDPE container vertically and allow for 500ml of the hydrogen charging solution to be poured into the top of the container followed by lowering of the lid, which submerged the end of the graphite electrode into the solution without contacting the wire. An external digital power supply was used to cathodically polarize the wire. By using the constant current mode of the power supply, the voltage between the wire and the graphite electrode varied based on the resistance of the solution and the changing surface area of the graphite electrode configured as an anode. With a selected current of 1 A and the known average accumulated charge for each grout condition, the polarization time was calculated for each grout condition. After each wire charging, the solution was poured back into the bulk solution, and the wire was removed from the bottom of the HDPE container and thoroughly wiped off to prevent any localized corrosion.

The reduction in ductility due to absorbed hydrogen was qualitatively assessed using the International Standard ISO 7801 reverse bend test and a constant load rate tensile test. The reverse bend test was performed using a custom set of vise grip inserts with a bending radius of 15 mm. A single steel wire was placed into the vise grip and secured to prevent unwanted movement. A lever arm was attached to the top of the wire and a rotation stop was secured to the bottom of the wire. The wire was subsequently bent back and forth, rotating 90 degrees initially and then 180 degrees for each consecutive bend until the wire fractured. The rate of bending was approximately two seconds for the first 90-degree bend and 4-5 seconds for the remaining 180-degree bends. The number of bends and the final position of the failure were recorded for each wire tested. Figure 5-1 shows a diagram of the reverse bending setup. While the

method provides an indication of the materials ductility, the result is only qualitative and is not an indication of the materials fracture strength.

Ideally, the stress strain characteristics of the charged specimens would be subjected to slow strain rate testing in which the wire is tensile tested under strain rates on the order of 10^{-5} mm/s. Such slow strain rates are required to allow the absorbed hydrogen to diffuse to defect sights during testing and to distinguish the mechanical performance between specimens of different absorbed hydrogen concentrations. Since such testing was not able to be performed in this work, prior testing reported in the literature on the same material and the resulting relationships between applied potential, solution pH, absorbed diffusible hydrogen content, and fracture initiation stress were used to assess the severity of the measured hydrogen and identify the potential implications of galvanic coupling to the embrittlement of prestressing steels within post-tensioned tendons.

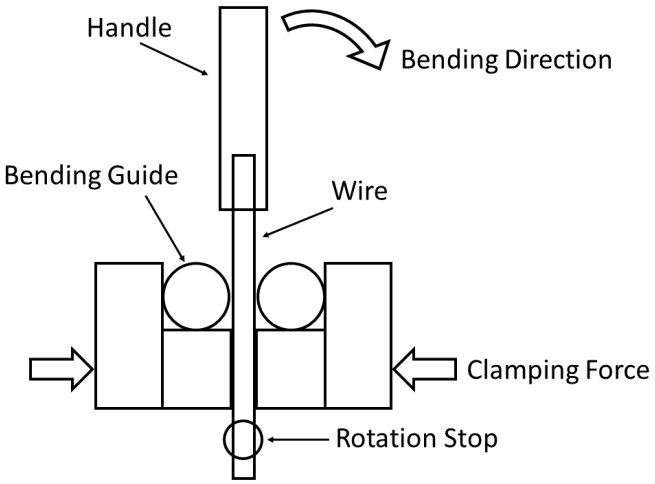

Figure 5-1. Diagram of reverse bending setup.

5.2 Grout Quality (Autopsy)

Tendon 1 was cast with the manufacturer's recommended water-to-cement ratio of 0.28 referred to as the good grout condition. During the autopsy, the grout was characterized as having a uniform porosity and uniform alkalinity. Figure 5-2 shows the section view of the grout in Tendon 1. The steel wire showed no signs of corrosion or visual signs of embrittlement. Figure 5-3 shows the inside view of the galvanized duct from Tendon 1. The inner wall of the galvanized duct was uniform in color and showed no signs of zinc corrosion or pitting.

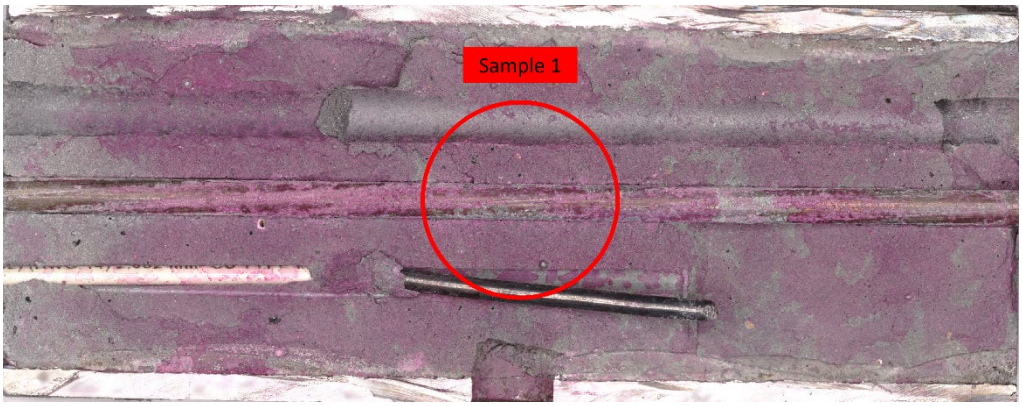

Figure 5-2. Section view of Tendon 1 cast with good grout (w/c = 0.28).


Figure 5-3. Inside view of the galvanized duct from Tendon 1 with good grout (w/c = 0.28).

Tendon 5 was cast with a 0.5 water-to-cement ratio which is almost double the recommended amount. This grout condition is referred to as the very soft condition. During the autopsy, the grout was characterized as having two distinct porosities and three distinct alkalinity zones. Importantly, a full void was identified in the upper 1/3 portion of the specimen observed as the left portion in Figure 5-4.

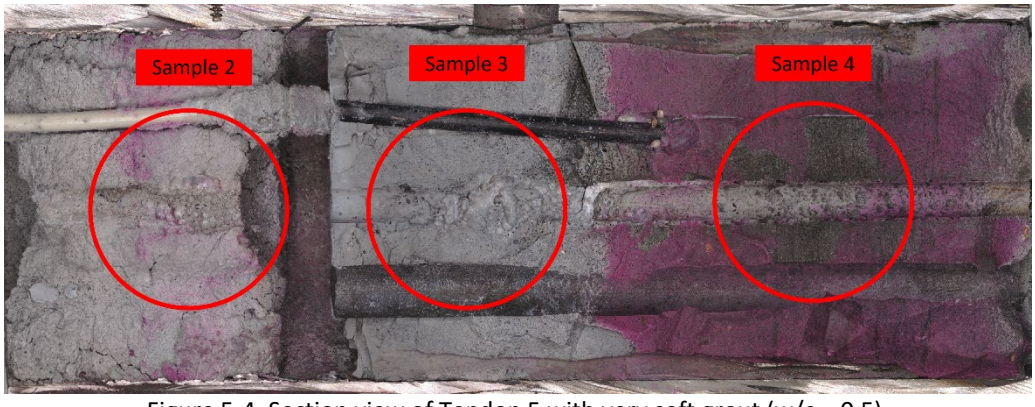

Figure 5-4. Section view of Tendon 5 with very soft grout (w/c = 0.5).

On the right side of Figure 5-4 (bottom of tendon), beneath the void, the grout was of similar porosity and density compared to the good grout in Tendon 1. However, on the left side of Figure 5-4 (top of tendon), above the void, the grout contained larger pores and was less dense compared to the grout at the bottom of tendon. Interestingly, the porous grout above the void did not easily propagate cracks initiated form the chisel during the autopsy and instead would crumble when a minimal force was applied to it. The alkalinity test showed a distinct band of low alkalinity in the center region of the wire, just below the void. The steel wire showed slight orange staining in the low alkaline region of the grout due possible due to corrosion. However, after bead blasting the surface of the wire, no significant corrosion pits were observed.

Figure 5-5 shows the inside view of the galvanized duct from Tendon 5. Three distinct zones were observed along the inner surface of the galvanized duct. On the right side of Figure 5-5 (bottom of tendon), the duct wall appeared darker in color corresponding with the size of the high alkaline grout band. The center zone of the duct was lighter in color and white zinc corrosion products can be seen along with minimal amounts of orange iron oxide. The left side of Figure 5-5 (top of tendon) shows a lighter color similar to the center zone but without the zinc and iron oxide products. From this it is clear that the low alkalinity region of the grout resulted in corrosion of the galvanized duct. The maximum corrosion penetration was measured using a 3D profilometer and was ~76 µm which corresponds to an approximate corrosion rate of 100 µm/yr. If it is assumed that such a high corrosion rate persists over time, corrosion through the thickness of the duct would occur in ~40-50 years. Further analysis of the grout in this region should provide more understanding of the potential cause of the corrosion.

Figure 5-5. Inside view of the galvanized duct from Tendon 5 with very soft grout (w/c = 0.5).

Tendon 7 was cast with an intermediate water to cement ratio of 0.38 referred to as the semisoft grout condition. During the autopsy, the grout was characterized as having three distinct porosities and three distinct alkalinity zones. Importantly, a partial void was identified in the center of the grout. Figure 5-6 shows the section view of the grout in Tendon 7.

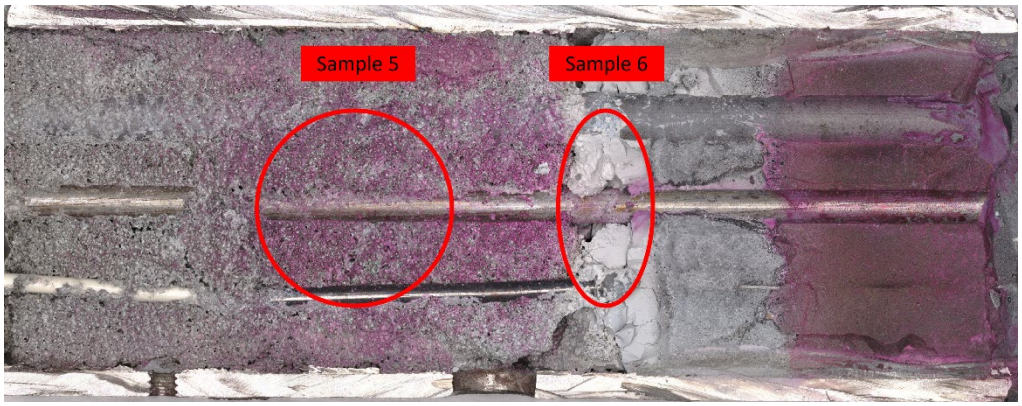

Figure 5-6. Section view of Tendon 7 with semisoft grout (w/c = 0.38).

On the right side of Figure 6 (bottom of tendon), beneath the partial void, the grout was of similar porosity and density compared to the good grout in Tendon 1 and the grout at the bottom of Tendon 5. In the center of Tendon 7, the grout was a lighter gray color and was of low strength. On the left side of Figure 5-6 (top of tendon), above the partial void, the grout contained larger pores similar to the grout at the top of tendon 5 and was less dense compared to the grout at the bottom of the tendon. Similar to the grout in the top of Tendon 5, the porous grout above the partial void did not easily propagate cracks initiated from the chisel during the autopsy and instead would crumble when a minimal force was applied to it. Further, the light gray grout in the center of the tendon was even weaker and would crumble when pinching with one's fingers. The alkalinity test showed a distinct band of low alkalinity in the center region of the wire, just below the partial void similar to Tendon 5. The steel wire also showed slight orange staining in the low alkaline region of the grout due to possible corrosion. However, after bead blasting the surface of the wire, no significant corrosion pits were found. Figure 5-7 shows the inside view of the galvanized duct from Tendon 7.


Figure 5-7. Inside view of the galvanized duct from Tendon 7 with semisoft grout (w/c = 0.38).

The inner wall of the galvanized duct from Tendon 7 showed three distinct zones. The center zone of the duct appears lighter in color and white zinc oxide can be seen along with moderate amounts of orange iron oxide corresponding to the size of the low alkaline grout band. On the left and right sides of Figure 5-7 (top and bottom of tendon), the duct wall appears lighter in color but without the zinc and iron oxide.

Tendon 10 was cast with the recommended water to cement ratio of 0.28 but the water was contaminated with 3.5% NaCl and is referred to as the NaCl grout condition. During the autopsy, the grout

was characterized as having a uniform porosity and uniform alkalinity. Figure 5-8 shows the section view of the grout in Tendon 10. The steel wire showed no signs of corrosion. Figure 5-9 shows the inside view of the galvanized duct from Tendon 10. The inner wall of the galvanized duct from the NaCl grout tendon showed areas of white zinc oxide throughout the length of the duct.

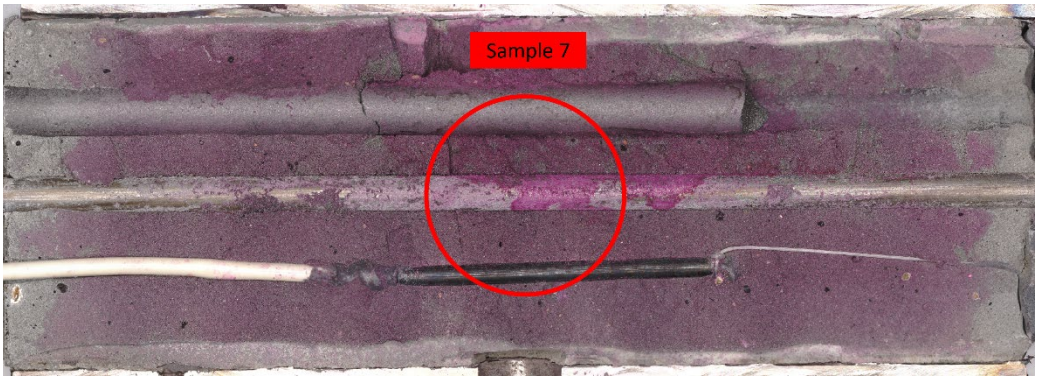

Figure 5-8: Section view of Tendon 10 made with grout mixed from a 3.5% NaCl by weight of water solution (w/c = 0.28).

Figure 5-9: Inside view of the galvanized duct from Tendon 10 made with grout mixed from a 3.5% NaCl by weight of water solution (w/c = 0.28).

Following the first batch of tendon autopsies, duplicate very soft grout, semisoft grout, and NaCl grout tendons were examined to confirm the results from the first batch. The duplicate tendons successfully confirmed the results found in the first batch of tendons. The adjacent grout pH and conductivity from extracted pore water values are shown in Table 6.

Table 6. Measured pH and conductivity from extracted pore water obtained from autopsied lab-cast tendons.

Sample	pH_1	pH_2	pH_3	$pH_{average}$	Conductivity ($\mu S/cm^2$)
1	12.15	12.15	12.15	12.15	2,402
2	10.99	10.98	10.98	10.98	1,137
3	9.81	9.85	9.82	9.83	1,702
4	12.29	12.28	12.28	12.28	3,121
5	11.99	11.98	11.98	11.98	1,774
6	10.68	10.64	10.63	10.65	1,872
7	11.98	11.98	11.97	11.98	3,041

The grout pore solution analysis results are presented in Table 7 for each sample with the sample number that corresponds to the designated location in the previous Figures. Samples 2-6 all had depleted levels of calcium, sodium, and potassium due to the higher water to grout mixing proportions. Generally, added mixing water exceeding the manufacturer's recommended amount resulted in higher sulfate concentrations and lower pH. The pH values presented however do not match the values obtained immediately after solution extraction possibly due to carbonation with the atmosphere despite ensure that the solution was sealed in airtight vials.

Table 7. Grout pore solution composition as determined by ICP-OES and IC.

Sample	Ca	Na	K	Cl^-	$SO4^{2-}$	pH
1	104.91	17.98	42.79	3.16	159.71	10.2
2	3.35	3.29	3.41	3.58	382.26	7.5
3	2.92	3.52	2.84	9.99	906.46	7.8
4	0.54	4.32	1.42	1.54	65.65	8
5	2.51	1.87	2.16	1.51	160.68	7.9
6	2.08	1.73	2.27	3.74	-	9.6
7	80.99	44.01	49.38	100.04	178.21	10.3

5.3 Hydrogen Absorption

The results from the hydrogen content analysis performed on segments of the steel wires from the first batch of tendons are shown in Table 8 along with the averaged accumulated galvanic charge passed for each grout condition during the testing period.

Table 8. Hydrogen concentration and average galvanic charged passed.

Sample ID	Sample Location	Exposure	Hydrogen Concentration (ppm)	Averaged Galvanic Charge Passed (Coulombs)
1	Good Grout Center	299	0.6	66.2
2	Very Soft Grout Top	270	0.6	1707.5
3	Very Soft Grout Middle	270	-	1707.5
4	Very Soft Grout Bottom	270	0.7	1707.5
5	Semisoft Grout Top	194	0.7	865.0
6	Semisoft Grout Center	194	0.6	865.0
7	NaCl Grout Center	135	0.9	210.0
8	Control Wire	-	0.6	-

The hydrogen concentration measured in the control wire was 0.6 ppm. Because the good grout wire measured the same 0.6 ppm, it can be reasonably assumed that there was no appreciable gain in hydrogen concentration due to the galvanic coupling when using the manufacturer's recommended water to cement ratio. In addition, the pH measured in the good grout was highly alkaline at 12.15 as expected. The very soft grout samples measured 0.6 ppm at the void with a pH of 10.98 in the top section and 0.7 ppm with a pH of 12.28 in the bottom section suggesting that the galvanic coupling may have been localized to the bottom region due to the presence of the void. The semisoft grout samples contained 0.7 ppm of absorbed hydrogen and a grout pore water solution of pH 11.98 in the top porous section and 0.6 ppm with a pH of 10.65 at the light gray low strength grout section. The NaCl grout measured 0.9 ppm with a pH of 11.98. Although this was the highest measured hydrogen content out of all the wires, it was only 0.3 ppm higher than the control wire.

5.4 Reverse-Bend Test

Since the steel wires from the first batch of tendons were sectioned for hydrogen concentration testing, the steel wires from the second batch were used to test the ductility of the steel for each condition using the reverse bending test. The results for this test are shown in Table 9. For a slow strain rate tensile test performed on a 16-inch-long king wire, with an approximate elongation 0.7 inches until failure, would take approximately 3 weeks to perform at a constant rate of 10^{-5} mm/s for a single specimen. To determine how subsurface hydrogen affects the tensile strength, the strain rate must be slow enough to allow the absorbed hydrogen to diffuse and propagate through the steel grain and reach the crack tip to facilitate brittle like fractures. An accelerated strain rate such as 10^{-4} mm/s will likely only show a ductile fracture of the wire, due to the slip planes of the laminal moving faster than the diffusion of absorbed hydrogen. Therefore, the reverse bending test was chosen due to time constraints to provide a quick assessment of any influence of the absorbed hydrogen. The results cannot be used as an indication of

fracture strength and since in some cases the galvanic coupling promoting hydrogen absorption was localized to regions of the wires due to grout segregation and void formation, it can be expected that there will be variability in the results.

Table 9. Reverse bending test results.

Sample Name	Number of Bends	Total Bending Angle (degrees)
Control King Wire 1	12	2205
Control King Wire 2	13	2385
Control King Wire 3	12	2190
Control King Wire 4	13	2385
1707C Charged in $H_2SO4 + Sb_2O_3$	2	405
1707C Charged in $H_2SO4 + Sb_2O_3$	2	375
1707C Charged in Sat. $Ca(OH)_2$	8	1455
1707C Charged in Sat. $Ca(OH)_2$	12	2160
Very Soft 1 – Tendon 3	9	1665
Semisoft 3 – Tendon 9	8	1485
NaCl 2 – Tendon 11	9	1665

The results of the reverse bend test performed on the control wires shows a repeatable 12-13 bends until failure. As an example of the worst-case scenario, four wires were cathodically polarized until the same accumulated charge that was recorded for the very soft grout condition tendons was achieved. Two of the wires were charged in a diluted sulfuric acid and a hydrogen recombination poison solution, and two wires were charged in a saturated calcium hydroxide pore water solution. The first two wires were charged at 1 A of current using a power supply that automatically varied the potential to achieve the desired current. This was done because as the charging was occurring, the counter electrode acted as a sacrificial anode that eroded over time. This change in surface area required a constantly changing potential to achieve a steady current. The results from these tests showed that a significant loss in ductility was achieved using the same charge experienced in the very soft grout tendons. When the solution was changed to the simulated pore water, the difference in solution conductivity resulted in a greater potential required to sustain 1 A of current. As the anode degraded, the resulting increase in voltage led to a limitation of the power supply and the constant current had to be reduced to 0.5 A. This continued until the applied potential again exceeded the power supply limit and the current was further reduced to 0.25 A. Finally, after the applied potential of the power supply reached its upper limit, the current was lowered to 0.2 A for the remaining of the charging. Each time when the current had to be lowered, the charging time had to be extended to achieve the same total charge. The result from this reverse bending test showed an intermediate value compared to the worse case diluted acid with recombination poison and the uncharged control wire. The second wire that was charged in the simulated pore water solution was set such that the constant current value was 0.2 A. After this charging was complete, the reverse bending test showed a similar result to the control wire. This may have been a result from the lower applied potential and the lower current. The results for the autopsied very soft, semisoft, and NaCl condition wires yielded less bends compared to the control king wires but more bends than the diluted acid with recombination poison. This shows that although the measured hydrogen concentrations for the very soft, semisoft, and NaCl condition wires only exceeded the control wire slightly, there was loss in ductility.

While this may be of concern, it does not suggest that the amount of absorbed hydrogen measured for the lab-cast tendons would result in premature failure.

5.5 Fracture Initiation Stress Estimates

With the galvanic potentials of the experimental tendons recorded directly after casting, an approximation of the subsurface concentration of hydrogen was made based on the experiments performed by Enos et. al. on a piece of type 1080 steel foil exhibiting a pearlitic drawn microstructure immersed in a saturated calcium hydroxide solution [8]. They determined a relationship for the steady state subsurface concentration of hydrogen (C_H) as a function of cathodic potential (η_{app}) where

$$log(C_H) = -6.50 - 6.4(\eta_{app}) \quad \text{Equation 5-1}$$

Using this relationship and the assumption that a cathodic potential of -900 mV_{SCE} is the minimum potential needed for the hydrogen evolution reaction to occur, the estimated concentration of subsurface hydrogen is 2-6 mol/cm^3 for the mild water tendons and 4-9 mol/cm^3 for the aggressive water tendons. While the subsurface hydrogen content does not reflect the total absorbed hydrogen, it is this value that determines the surface fracture initiation stress. Further crack propagation may depend on the distribution of absorbed hydrogen both radially and longitudinally through the steel wires.

To predict the impact on the mechanical performance of the steel strands as the concentration of subsurface hydrogen increased, Enos et. al. established a relationship of the local fracture initiation stress (σ_i) as a function of subsurface hydrogen concentration (C_H) where

$$\sigma_i = 2{,}599 - 231.5\, log(C_H/5.0 \times 10^{-7}) \quad \text{Equation 5-2}$$

If it is assumed that the total absorbed hydrogen measured is equal to the diffusible hydrogen, sample 6 obtained from the NaCl contaminated specimen that showed the largest amount of hydrogen (0.9 ppm) would only result in a ~2% decrease in fracture initiation stress. This suggest that the amount of hydrogen absorbed during the initial curing of the grout even for the most severe conditions would not cause sufficient hydrogen absorption for premature failure.

The estimated local fracture initiation stress of a single steel wire that was surrounded with highly conductive mild or aggressive water, was reduced to 1025 MPa and 925 MPa respectively. This is a significant reduction compared to the uncharged local fracture initiation stress of ~2600 MPa estimated by Enos et. al. [8]. A reduction in initiation stress of this magnitude is significant because, assuming that tendons are stressed to 80% of their guaranteed ultimate tensile stress (~1480 MPa) when being placed [7], then relaxed to 70% of their guaranteed ultimate tensile stress (~1295 MPa) after grouting [7], the estimated local fracture initiation stress is below the residual tensile stress that will lead to fracture of the affected strands. Because of the assumptions made when determining these estimates, further work will be required to confirm or improve the relationships between galvanic potential, hydrogen content, and mechanical properties of the steel strands.

Under an unlikely extreme condition of rainwater or seawater somehow filling a voided duct, galvanic coupling is promoted due to the conductivity of the solution. From the results of the galvanic coupling experiments presented in deliverable 3, in a mild and aggressive solution the steady state potential reached after 1 week of exposure was ~ -1000 V_{SCE} and ~-1050 $V_{SCE,}$ respectively. There was no indication

that the potential would become more positive provided extended exposure time. Based on these values, the steady state subsurface hydrogen concentration can be estimated according to Enos et al.[44] as

$$\log(C_H) = -6.753 - 2.976(\eta_{app}) \quad \text{Equation 5-3}$$

This is an empirical expression developed from experiments performed on a piece of 1080 steel foil exhibiting a pearlitic drawn microstructure immersed in simulated ocean water [8]. The term η_{app} represents the difference between the applied potential and the hydrogen evolution reversible potential which is dependent on solution pH and can be estimated according to

$$E_{H+/H} = -0.241V_{SCE} - 0.059pH \quad \text{Equation 5-4}$$

As the pH increases, the hydrogen reversible potential becomes more negative making it more difficult to evolve hydrogen under cathodic potentials. While the amount of hydrogen evolved can be expected to be greater in mild and aggressive water than in typical grout conditions, the amount of hydrogen absorbed should be less since there is not much calcium hydroxide which prevents hydrogen recombination. Combining these equations, one can estimate the reduction in fraction initiation stress given an applied overpotential and the pH of the medium.

The percent reduction in fracture initiation stress is presented in Table 10 for each condition according to the maximum galvanic potential measured. The estimates provided consider the most negative potential recorded for each grout condition and since the potential quickly becomes more positive as the grout cures, it is likely that these are greatly overestimated. Nevertheless, the values provide a sense of severity considering the worst-case scenario for fully grouted tendons in which the greatly negative potentials would be sustained over a considerable period of time. The values estimated for the mild and aggressive water solutions representative of an extreme case of grout voids with water intrusion are expected to be realistic estimates. A 20-23% reduction in fracture initiation stress may not cause brittle failure under typical loading conditions in which the wires are stressed to approximately 1295 MPa after relaxation but if there any preexisting surface defects or corrosion pits that sufficiently reduce the cross-sectional area of the wire, then failure is possible. Nevertheless, galvanic coupling by itself does not seem to be substantial enough to cause failure on its own.

Table 10. Estimated strength reduction based on pH and max measured cathodic potential.

	Erev	V_{max}	η_{app}	Est. Ch(ppm)	σ_i, MPa	% Reduction
Good	-0.957	-	0	0	2600	0
Very soft	-0.888	-1.124	-0.235	14	2268	13
Very soft	-0.965	-1.124	-0.158	4	2391	8
soft	-0.947	-1.094	-0.146	3	2411	7
soft	-0.869	-1.094	-0.224	12	2285	12
NaCl	-0.947	-.975	-0.027	0.5	2600	0
Mild water	-0.654	-1.05	-0.396	80	2090	20
Aggressive water	-0.654	-1.08	-0.426	177	2010	23

5.6 Summary

In this chapter, autopsies of the single wire mock tendons were performed to assess the condition of the grout and the galvanized steel ducts for each grout condition tested. The grout was analyzed visually for indication of segregation and voids, and its composition was identified for several regions. The semisoft and very soft grout mixes resulted in regions of grout that were low in pH and high in sulfate concentration. Within these regions, the galvanized steel duct was observed to have substantial corrosion damage that is expected to result in a more negative corrosion potential and likely promote galvanic activity. Because this occurred on a local scale, the measurements may not have been sensitive to it because they reflect a surface averaged result. Duct corrosion was also observed with the chloride-contaminated grout tendon.

The steel wire in each case was analyzed for hydrogen content at locations that correlated to specific grout features. The amount of hydrogen absorbed was minimal in each case, but the most was found in the chloride-contaminated grout even though the very soft grout produced the most galvanic coupling. The very soft grout had a much lower calcium content than both the chloride-contaminated and good grout conditions, suggesting that there is less calcium hydroxide to act as a hydrogen recombination poison.

A series of reverse bend tests were performed on either control, charged, or extracted wires. The bend tests were capable of distinguishing between various charging conditions according to the number of bends required to fracture the steel. These tests were used to provide an assessment of the influence of the absorbed hydrogen on the strain-hardening capacity of the steel. Uncharged wires required at least 12 bends to fracture while wires charged in sulfuric acid containing antimony trioxide as a strong recombination poison only required two. Wires charged with hydrogen in calcium hydroxide resulted in an intermediate ductility response requiring eight bends to fracture.

Based on the testing performed over a limited time frame, the galvanic coupling induced under various grout conditions did not result in a substantial amount of absorbed hydrogen that would be expected to cause severe embrittlement and subsequent failure under typical loading conditions. While the experiments performed represent a limited dataset, the knowledge of the influencing parameters on the production and absorption of hydrogen allows one to assess the susceptibility of hydrogen embrittlement considering the level of galvanic coupling between the wires and the duct. The wires extracted from the experimental tendons within the chloride-contaminated or soft grout required eight or nine bends. While the results provide some indication of ductility based on exposure condition, they cannot be used to suggest that the amount of hydrogen absorbed would result in fracture.

To estimate the reduction in fracture initiation stress for each condition, the measured pH was used to identify the hydrogen reversible potential. From the measured maximum corrosion galvanic potential, an overpotential was calculated which was used to estimate the subsurface concentration of hydrogen. The estimates were much more than the measured amount of hydrogen in the extracted wires because the extracted wires only experience the maximum potential soon after casting, and these calculations assume steady state conditions. According to the estimates, if the galvanic potential remained at the maximum values, the very soft grout condition could result in as much as a 13% reduction in fracture initiation stress, while the semisoft could reach a reduction of ~12%. This amount of reduction in fracture strength would not necessarily result in fracture under typical loading conditions unless flaws such as corrosion pits or

surface cracks are present that result in stress concentrations sufficient to exceed the fracture initiation stress.

6 Conclusions

Testing was performed to identify the susceptibility of prestressing steel strands contained within galvanized steel ducts to hydrogen embrittlement considering grout condition. As a first step, a failure analysis was performed on fractured strands obtained from the Wando River Bridge to identify whether hydrogen embrittlement played a role. Following this, experiments were performed to quantify the level of galvanic activity considering ideal and unanticipated grout conditions. Data obtained from the experiments were used to simulate galvanic activity in an idealized tendon geometry to provide context to the experimental results. Autopsies were then performed to characterize the condition of the grout and measure the absorbed hydrogen concentration of the steel wires. Mechanical testing and theoretical estimates of reduction in strength were used to describe the implications of galvanic coupling between prestressing steel strands and galvanized steel ducts on mechanical performance.

The conclusions from this report include the following:

6.1 Wando River Tendon Failure

Based on the results of this report and those of the failure analysis of the Wando River Bridge strands, the most likely cause of failure as well as the source of hydrogen was localized corrosion of the strand within grout voids of the duct. Under these conditions and depending on the relative humidity within the duct, atmospheric corrosion of the strands can result in hydrogen absorption under corrosion product layers (as shown in[48]) further exacerbating the issue. Future research should be performed to assess the mechanical properties of corroded prestressing steel strands accounting for absorbed hydrogen using slow strain rate testing to determine the likelihood of strand failure.

6.2 Galvanic Coupling

The amount of galvanic coupling between the steel strands and the galvanized steel duct is influenced by many parameters which include the grout resistivity, the proximity of the steel to the duct, the relative surface area of steel to the duct, and the kinetics of each material resulting from the condition of the grout. If the grout manufacturer's recommended water to cement ratio is followed and potable water is used, the resulting galvanic activity is not sufficient to increase the hydrogen content of the steel wire. Otherwise, if increased water or salt contaminated water is used, the wires may be polarized to substantially negative potentials to promote hydrogen evolution at least during the grout setting period. This conclusion is specific to the grout tested in this work as other grout formulations may have different hydration behaviors.

A substantial increase (~35% or greater) in the water to cement ratio of the grout used in this work caused distinct regions of varying pH and voids. Regions of low pH grout corresponded to locations of substantial corrosion of the galvanized duct. Under such conditions, the corrosion potential of the duct would become increasingly negative further polarizing the wire to more cathodic potentials and therefore promoting hydrogen evolution. Evaluation techniques capable of assessing grout condition of internal tendons is required to ensure such conditions are not present.

Based on the experiments and the simulations performed, the current density associated with the hydrogen evolution reaction may be as high as 2.5 $\mu A/cm^2$ for a 20-strand tendon with a 3-inch-diameter duct assuming the strands are at least 0.5 cm away from the duct. The current density will increase as the strand becomes closer to the duct.

6.3 Hydrogen Absorption

The chloride-contaminated grout condition resulted in the most measured hydrogen content with values of 0.3 ppm greater than the controls despite experiencing a much lower accumulated charge of ~200 C versus 1700 C for the very soft grout condition. While this is just a single result that needs to be verified with replicate data, one potential reason for this is the higher concentration of calcium hydroxide in the chloride-contaminated grout. Calcium hydroxide promotes hydrogen absorption since it acts as a hydrogen recombination poison. Therefore, while the very soft grout condition resulted in the most galvanic activity it was not the greatest promoter of hydrogen absorption.

6.4 Implications to Mechanical Properties

Reverse bending tests of the autopsied steel wires showed some loss in ductility compared to the control wires. However, these tests cannot be used to determine reduction in fracture strength. Based on the relationship developed by Enos et al. [44] considering saturated calcium hydroxide solutions, the measured amount of hydrogen absorbed (0.9ppm) would only result in a 2% decrease in fracture strength. While slow-strain rate testing should be performed to confirm this, it is likely that galvanic coupling promoted by early grout conditions during the curing stage will not result in substantial hydrogen embrittlement of prestressing steel wires within galvanized steel ducts. Whether hydrogen embrittlement is of concern for longer exposure times depends on the availability of oxygen within the tendon. Future work is required to determine whether oxygen depletion in post-tensioned tendons is a possibility.

Based on the conclusions outlined here, the following recommendations are provided.

1) The grout needs to be mixed and placed in accordance with the manufacturer's recommendations to avoid grout segregation and voids.
2) It should be ensured that the tendons are properly sealed to prevent any water intrusion. If this cannot be ensured, an alternative duct material should be considered.

7 Future Research Needs

While the analysis reported in this work has provided key insight into the severity of galvanic coupling, there are questions that remain which are stated below as potential directions for future research:

7.1 Possibility of Oxygen Depletion

The amount of hydrogen absorbed for the tests performed in this work are due to the early effects of hydration of the grout and may not reflect long term exposure conditions. One potential concern is that oxygen within the tendon could be depleted resulting in a more negative potential applied to the steel that would promote hydrogen evolution. While the interstices of the steel strands may provide a readily available oxygen reserve, this would need to be confirmed with testing. Results are presented in Figure 7-1 of preliminary simulations aimed at assessing the possibility of oxygen depletion considering the availability of oxygen within the interstitial space of the steel strands. While the assumed availability of oxygen through the wires of the strands prevents complete oxygen depletion there is still enough oxygen depletion to cause of reduction in steel potential and therefore an increase in the rate of hydrogen evolution. These results are preliminary and while based on the kinetic data obtained in this work, further experiments are required to understand the diffusivity of oxygen in grout considering the different conditions and the ability of oxygen to pass through the interstitials of the strands.

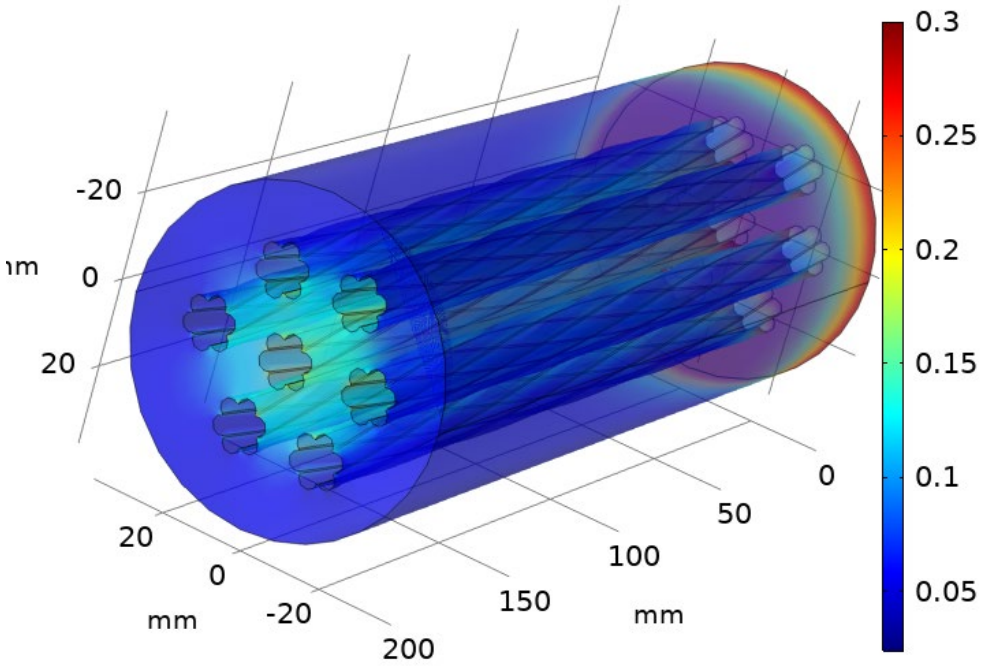

Figure 7-1 Distribution of steady state oxygen concentration considering oxygen flux through the interstitial space of the stands. Dark blue represents a concentration of zero while dark red represents oxygen saturation.

7.2 The Susceptibility of Corrosion Induced Cracking

Regarding the Wando River Bridge, the failures seem to be a result of grout voids resulting in early onset corrosion and significant loss of cross-sectional area that may have facilitated by earlier hydrogen absorption. Based on the soft grout experiments performed in this work, it may be that the added water greatly exceeded the recommended amount during placement that may have resulted in bleed water evaporation resulting in void formation and low pH grout regions. The low pH grout, which was found to have high sulfate content as reported in this work and elsewhere, was shown to cause corrosion of the galvanized steel duct. Additionally, it is likely that moisture or water infiltration within the voided regions of the ducts caused severe corrosion of the strands that resulted in hydrogen absorption and embrittlement. However, future work is required to identify the specific conditions required to cause corrosion induced hydrogen absorption in voided ducts and the mechanical property implications. In a recent paper, it was shown that hydrogen may be absorbed by prestressing steel under specific corrosion products. Current failure projection models, of post-tensioned tendons only consider reduction in strength due to reduction in cross-sectional area and do not consider whether hydrogen absorption is contributing to reduced mechanical function.

To address this, it is recommended that research be performed to first identify the conditions that promote corrosion induced hydrogen absorption and the implications to tendon durability. This may be achieved by simulating the voided atmosphere of internal tendons using environmental chambers in which temperature and humidity is controlled. Under the controlled conditions, the amount of hydrogen absorption can be tracked as the steel corrodes by relating the hydrogen content to the distribution of surface work function measured with a microscopic scanning kelvin probe.

Slow-strain rate tests (SSRT) or constant extension rate tests (CERT) on the corrosion damaged strands could then be performed to assess the potential for corrosion induced cracking of the strands. These tests are typically performed under a strain rate of 10^{-6} mm/s which allows time for absorbed hydrogen to diffuse to lattice imperfections causing embrittlement. The results of this study would provide a detailed assessment of the role of voids in tendon durability and whether a minimum void size should be specified.

7.3 Implications to Corrosion Mitigation Strategies

Tendon impregnation has been considered and implemented on a limited basis as a corrosion mitigation strategy for post-tensioned tendons. This method involves pressure-injecting a corrosion mitigating fluid through the interstitial spaces of the steel strands to coat the steel in an effort to prevent corrosion and or reduce the rate of ongoing corrosion. If grout deficiencies are present either in the form of large voids or grout segregation this may influence the ability of the strategy to adequately prevent corrosion. The suitability of this method for internal tendons containing galvanized steel ducts needs to be evaluated.

References

[1] C. L. Alexander, Y. Chen, and M. E. Orazem, "Impedance-Based Detection of Corrosion in Post-Tensioned Cables: Phase 2 from Concept to Application," FDOT Final Report BDV31-977-35, University of Florida, Gainesville, FL, 2017.

[2] S. Adcox, "DOT: Corrosion 'exploded' cable in Wando Bridge," in *The Post and Courier*, ed. Charleston, SC, 2018.

[3] J. N. Steinhoff, Maciejewski, "Metallurgical Failure Analysis of a Bridge Post-Tensioning Tendon," Applied Technical Services, Inc., Marietta, GA, 2018.

[4] A. A. Sagues, "Hydrogen Content Evaluation, Wando River Tendon Strand Samples, Report to Florida Department of Transportation," University of South Florida, Tampa, FL, 2018.

[5] O. Barrera *et al.*, "Understanding and mitigating hydrogen embrittlement of steels: a review of experimental, modelling and design progress from atomistic to continuum," *Journal of Materials Science,* Review vol. 53, no. 9, pp. 6251-6290, 2018, doi: 10.1007/s10853-017-1978-5.

[6] S. Thomas, G. Sundararajan, P. D. White, and N. Birbilis, "The Effect of Absorbed Hydrogen on the Corrosion of Steels: Review, Discussion, and Implications," *Corrosion,* vol. 73, no. 4, pp. 426-436, 2017, doi: 10.5006/2242.

[7] J. Toribio, "HELP versus HEDE in progressively cold-drawn pearlitic steels: Between Donatello and Michelangelo," *Engineering Failure Analysis,* vol. 94, pp. 157-164, 2018/12/01/ 2018, doi: https://doi.org/10.1016/j.engfailanal.2018.07.026.

[8] M. Schupack and M. G. Suarez, "Some recent corrosion embrittlement failures of prestressing systems in the United States," *Journal - Prestressed Concrete Institute,* Article vol. 27, no. 2, pp. 38-55, 1982. [Online]. Available: https://www.scopus.com/inward/record.uri?eid=2-s2.0-0020101821&partnerID=40&md5=56aad38bc2e321f5c6cfd7183b195254.

[9] A. Moreton, "Performance of segmental and posttensioned bridges in Europe," *Journal of Bridge Engineering,* Article vol. 6, no. 6, pp. 543-555, 2001, doi: 10.1061/(ASCE)1084-0702(2001)6:6(543).

[10] B. Isecke, "COLLAPSE OF THE BERLIN CONGRESS HALL PRESTRESSED CONCRETE ROOF," *Materials Performance,* Article vol. 21, no. 12, pp. 36-39, 1982. [Online]. Available: https://www.scopus.com/inward/record.uri?eid=2-s2.0-0020296902&partnerID=40&md5=fc53990e067be7ab63720efb10c72d85.

[11] R. Helmerich and A. Zunkel, "Partial collapse of the Berlin Congress Hall on May 21st, 1980," *Engineering Failure Analysis,* vol. 43, pp. 107-119, 2014/08/01/ 2014, doi: https://doi.org/10.1016/j.engfailanal.2013.11.013.

[12] Siva Corrosion Services Inc., "I-526 James B. Edwards Bridge over the Wando River in Charleston, SC: FAILED TENDON INVESTIGATION," 100128-02, West Chester, PA, 2017.

[13] X. Sauvage, X. Quelennec, J. J. Malandain, and P. Pareige, "Nanostructure of a cold drawn tempered martensitic steel," *Scripta Materialia,* vol. 54, no. 6, pp. 1099-1103, 2006/03/01/ 2006, doi: https://doi.org/10.1016/j.scriptamat.2005.11.068.

[14] M. Elices, "Influence of residual stresses in the performance of cold-drawn pearlitic wires," *Journal of Materials Science,* Article vol. 39, no. 12, pp. 3889-3899, 2004, doi: 10.1023/B:JMSC.0000031470.31354.b5.

[15] J. Toribio and E. Ovejero, "Composite microstructure of cold-drawn pearlitic steel and its role in stress corrosion behavior," *Journal of Materials Engineering and Performance,* vol. 9, no. 3, pp. 272-279, 2000/06/01 2000, doi: 10.1361/105994900770345917.

[16] J. Toribio, B. González, and J. C. Matos, "Microstructure and mechanical properties in progressively drawn pearlitic steel," *Materials Transactions,* Article vol. 55, no. 1, pp. 93-98, 2014, doi: 10.2320/matertrans.MA201316.

[17] J. Toribio, M. Lorenzo, D. Vergara, and V. Kharin, "Influence of the die geometry on the hydrogen embrittlement susceptibility of cold drawn wires," *Engineering Failure Analysis,* Article vol. 36, pp. 215-225, 2014, doi: 10.1016/j.engfailanal.2013.10.010.

[18] *Standard Specification for Low-Relaxation, Seven-Wire Steel Strand for Prestressed Concrete*, A. A. A416M-18, ASTM International, Online, 2018.

[19] J. Toribio, M. Lorenzo, D. Vergara, and V. Kharin, "Hydrogen Embrittlement of Cold Drawn Prestressing Steels: the Role of the Die Inlet Angle," *Materials Science,* vol. 49, no. 2, pp. 226-233, 2013/09/01 2013, doi: 10.1007/s11003-013-9603-5.

[20] W. H. Johnson, "On Some Remarkable Changes Produced in Iron and Steel by the Action of Hydrogen and Acids," *Nature,* vol. 11, no. 281, pp. 393-393, 1875/03/01 1875, doi: 10.1038/011393a0.

[21] S. Lynch, "Hydrogen embrittlement phenomena and mechanisms," *Corrosion Reviews,* Review vol. 30, no. 3-4, pp. 105-123, 2012, doi: 10.1515/corrrev-2012-0502.

[22] E. McCafferty, *Introduction to corrosion science* (Introduction to Corrosion Science). Springer, NY, 2010.

[23] T. Hajilou, "Hydrogen-Assisted Cracking Investigated by In Situ Electrochemical Micro-Cantilever Bending Test," Norwegian University of Science and Technology, Norway, 2018.

[24] J. Toribio, "Role of hydrostatic stress in hydrogen diffusion in pearlitic steel," *Journal of Materials Science,* Article vol. 28, no. 9, pp. 2289-2298, 1993, doi: 10.1007/BF01151655.

[25] L. B. Pfeil, "The effect of occluded hydrogen on the tensile strength of iron," *Proceedings of the Royal Society of London. Series A, Containing Papers of a Mathematical and Physical Character,* vol. 112, pp. 182-195, 1926.

[26] C. D. Beachem, "A new model for hydrogen-assisted cracking (hydrogen "embrittlement")," *Metallurgical Transactions,* Article vol. 3, no. 2, pp. 441-455, 1972, doi: 10.1007/BF02642048.

[27] M. Nagumo, "Hydrogen related failure of steels - A new aspect," *Materials Science and Technology,* Review vol. 20, no. 8, pp. 940-950, 2004, doi: 10.1179/026708304225019687.

[28] T. Neeraj, R. Srinivasan, and J. Li, "Hydrogen embrittlement of ferritic steels: Observations on deformation microstructure, nanoscale dimples and failure by nanovoiding," *Acta Materialia,* Article vol. 60, no. 13-14, pp. 5160-5171, 2012, doi: 10.1016/j.actamat.2012.06.014.

[29] R. Konno, T. Manabe, N. Matsui, D. Hirakami, and K. Takai. *Factors causing hydrogen embrittlement of cold-drawn pearlitic steel fractured under elastic/plastic region, Minerals Metals and Materials Series*, vol. Part F6, pp. 579-586, 2017.

[30] D. A. Indeitsev, E. V. Osipova, and V. A. Polyanskiy, "A statistical model of hydrogen-induced fracture of metals," *Doklady Physics,* Article vol. 59, no. 11, pp. 534-538, 2014, doi: 10.1134/S1028335814110093.

[31] D. G. Enos and J. R. Scully, "A critical-strain criterion for hydrogen embrittlement of cold-drawn, ultrafine pearlitic steel," *Metallurgical and Materials Transactions A: Physical Metallurgy and Materials Science,* Article vol. 33, no. 4, pp. 1151-1166, 2002, Art no. 217, doi: 10.1007/s11661-002-0217-z.

[32] D. G. Enos, A. J. Williams Jr, G. G. Clemeña, and J. R. Scully, "Impressed-Current Cathodic Protection of Steel-Reinforced Concrete Pilings: Protection Criteria and the Threshold for Hydrogen Embrittlement," *Corrosion,* Article vol. 54, no. 5, pp. 389-402, 1998, doi: 10.5006/1.3284867.

[33] W. H. Hartt, C. C. Kumria, and R. J. Kessler, "Influence of potential, chlorides, pH, and precharging time on embrittlement of cathodically polarized prestressing steel," *Corrosion,* Article vol. 49, no. 5, pp. 377-385, 1993, doi: 10.5006/1.3316064.

[34] M. H. Joseph Fernandez, Alberto A. Sagüés, Gray Mullins, "Corrosion characteristics of unprotected post-tensioning strands under stress," University of South Florida, Tampa, FL, 2014.

[35] R. M. S. Pereira, "Accelerated Corrosion Testing, Evaluation and Durability Design of Bonded Post-Tensioned Concrete Tendons," The University of Texas at Austin, 2003.

[36] J. S. West, J. E. Breen, and R. P. Vignos, "Evaluation of corrosion protection for internal prestressing tendons in precast segmental bridges," *PCI Journal,* Article vol. 47, no. 5, pp. 76-91, 2002, doi: 10.15554/pcij.09012002.76.91.

[37] J. Mietz, A. Burkert, J. Lehmann, A. Burkert, and G. Eich, "Galvanised constructional elements in contact with prestressing steel tendons," *Materials and Corrosion,* Article vol. 59, no. 2, pp. 131-138, 2008, doi: 10.1002/maco.200804114.

[38] J. G. Yu, J. L. Luo, and P. R. Norton, "Electrochemical investigation of the effects of hydrogen on the stability of the passive film on iron," *Electrochimica Acta,* vol. 47, no. 10, pp. 1527-1536, 2002/03/01/ 2002, doi: https://doi.org/10.1016/S0013-4686(01)00882-9.

[39] S. Adcox, "DOT: Cossosion 'exploded' cable in Wando Bridge, sending grout flying 100 feet.," The Post and Courier, Charleston, S.C., 2018.

[40] S. C. S. Inc., "I-526 James. B Edwards Bridge over the Wando River in Charleston, SC: Failed Tendon Investagation," Charleston, 2017.

[41] HDR, "I-526 Wando River Bridge Post-Tensioning Evalustion," Charleston, 2018.

[42] N. Steinhoff and j. Maciejewski, "Metallurgical Failure Analysis of a Bridge Post-Tensioning Tendon.," Applied Technical Services, INC., 2018.

[43] A. A. Sagues, "Hydrogen Content Evaluation, Wando River Tendon Strand Samples.," Florida Department of Transportation, Tampa, 2018.

[44] D. G. Enos, A. J. Williams Jr, and J. R. Scully, "Long-Term Effects of Cathodic Protection on Prestressing Concrete Structures: Hydrogen Embrittlement of Prestressing Steel," *Corrosion,* vol. 53, no. 11, pp. 891-908, 1997.

[45] W. H. Hartt and S.-K. Lee, "Projecting Corrosion-Induced Bridge Tendon Failure Resulting from Dificent Grout: Part I-Model Development and Example Results," *Corrosion,* vol. 72, no. 8, pp. 991-997, 2016.

[46] C.-H. Jeon, C. D. Nguyen, and C.-S. Shim, "Assessment of Mechanical Properties of Corroded Prestressing Strands," *Applied Sciences,* vol. 10, pp. 1-19, 2020.

[47] E. Akiyama, K. Matsukado, M. Wang, and K. Tsuzaki, "Evaluation of hydorgen entry into high strength steel under atmospheric corrosion," *Corrosion Science* vol. 52, pp. 2758-2765, 2010.

[48] D. Rudomilova, T. Prošek, and M. Ström, "Hydrogen Entry into Steel Under Corrosion Products," *Corrosion Journal,* vol. 77, no. 4, pp. 427-432, 2021.